# Title: An optogenetic toolkit for robust activation of FGF, BMP, & Nodal signaling in zebrafish

**Running title:** Optogenetic signaling activation

**Key words:** molecular optogenetics, zebrafish, signaling, FGF, BMP, Nodal, embryogenesis

Leanne E. Iannucci[1†], Velanganni Selvaraj Maria Thomas[1†], Micaela R. Murphy[1], Caitlin E.T. Donahue[1], William K. Anderson[1], Catherine E. Rogers[1], Allison J. Saul[1,2], Katherine W. Rogers[1*]

[†]These authors contributed equally

[1]Unit on Developmental Signaling, Division of Developmental Biology, *Eunice Kennedy Shriver* National Institute of Child Health and Human Development, NIH, Bethesda, MD 20814, USA

[2]Current address: School of Biological Sciences, University of Utah, Salt Lake City, UT 84112, USA

[*]Correspondence: katherine.rogers@nih.gov

**ABSTRACT** Cell signaling regulates a wide range of biological processes including development, homeostasis, and disease. Accessible technologies to precisely manipulate signaling have important applications in basic and translational research. Here, we introduce an optogenetic toolkit comprised of 1) a zebrafish-optimized FGF signaling activator, 2) a single-transcript Nodal signaling activator, and 3) a previously established BMP signaling activator. We thoroughly characterize this suite of tools in zebrafish embryos and show that they provide tunable, light-dependent spatiotemporal control of signaling *in vivo*. In response to blue light (~455 nm), receptor kinase domains fused to blue light-dimerizing LOV domains enable robust signaling activation with minimal ectopic activity in the dark or at wavelengths over 495 nm. Optogenetic activation by each tool is pathway-specific and results in increased expression of known target genes. Signaling is activated with rapid on/off kinetics, and activation strength depends on light irradiance. Finally, we demonstrate spatially localized signaling activation with our optimized FGF activator. Together, our results establish this optogenetic toolkit as a potent experimental platform to rapidly, directly, and adjustably activate FGF, BMP, and Nodal signaling in zebrafish embryos.

## INTRODUCTION

Many biological processes are regulated by cell signaling, from development to homeostasis to disease. Signaling dynamics (i.e., levels and durations) play a crucial role in orchestrating diverse biological processes including embryonic patterning (Bosman and Sonnen, 2022; Hill, 2022; Kicheva and Briscoe, 2023; Sagner and Briscoe, 2017). For example, cell fate decisions can differ dramatically based on a single pathway's signaling frequency (Purvis and Lahav, 2013). Spatiotemporally dynamic signaling gradients in developing tissues are known to coordinate patterning in multiple contexts across the animal kingdom (Guillotin and Birnbaum, 2020; Hill, 2022; Jones and Mullins, 2022; Liberali and Schier, 2024; Sagner and Briscoe, 2017). During early vertebrate development, dynamic signaling gradients generated by fibroblast growth factor (FGF), bone morphogenetic protein (BMP), and Nodal are established (Hill, 2022; Jones and Mullins, 2022; Liberali and Schier, 2024). These pathways signal via receptor kinases and remain at the center of many active developmental biology investigations due to their key roles in patterning the embryonic body axes. Established methods to manipulate FGF, BMP, and Nodal signaling such as mutating pathway genes, using heat shock promoters to drive genetically encoded agonists or antagonists, recombinant proteins, and small molecule drugs have provided foundational information about their roles. However, these methods can be cumbersome and slow. Precision molecular technologies to experimentally activate receptor kinase-based signaling *in vivo* can open new avenues of study.

Molecular optogenetic strategies use light to manipulate biological processes and have yielded novel insights across fields including developmental biology (Johnson and Toettcher, 2018; Rogers and Müller, 2020). Optogenetics has been used to control processes as diverse as gene expression (LaBelle et al., 2021; Reade et al., 2017), apoptosis (Mruk et al., 2020), protein localization (Buckley, 2019; Buckley et al., 2016), and signaling (Benman et al., 2022; Čapek et al., 2019; Kainrath et al., 2017; McNamara et al., 2025; Rogers et al., 2020; Sako et al., 2016; Saul, Rogers et al., 2023). This technology has generated considerable enthusiasm, reflected in the nearly exponential increase in publications involving molecular optogenetic approaches since the early 2000s (Kolar et al., 2018). Research exploring signaling is well suited for molecular optogenetic approaches because this technology can enable precise spatiotemporal control over signaling (Farahani et al., 2021). Applying these strategies to experimentally manipulate FGF, BMP, and Nodal signaling in vertebrate embryos is appealing because optogenetic methods to

activate receptor kinase-regulated pathways such as these have been demonstrated (Chang et al., 2014; Crossman and Janovjak, 2022; Grusch et al., 2014; Humphreys et al., 2020; Kainrath et al., 2017; Kim et al., 2014; McNamara et al., 2025; Rogers et al., 2020; Sako et al., 2016).

Optogenetic tools have already helped reveal key insights into the roles of signaling in development across a range of model systems (Farahani et al., 2021; Rogers and Müller, 2020), including the vertebrate zebrafish embryo. This widely used model is well suited to address many developmental biology questions because it is externally fertilized, translucent, and microscopy-friendly (Hill, 2022; Jones and Mullins, 2022; Liberali and Schier, 2024; Mullins et al., 2021)—all attributes that make zebrafish an ideal system for optogenetic approaches. Optogenetic manipulation of Nodal signaling in zebrafish has been used to define developmental windows during which Nodal is actively patterning the germ layers (Reade et al., 2017; Vopalensky et al., 2018), to investigate how Nodal and BMP signaling are interpreted (Rogers et al., 2020; Sako et al., 2016), and to examine the spatial requirements for Nodal-mediated patterning (McNamara et al., 2025). Optogenetic approaches have also provided insights into how Nodal and non-canonical Wnt signaling influence cell migration in zebrafish embryos (Čapek et al., 2019; Emig et al., 2024). Finally, optogenetic tools that activate extracellular signal-regulated kinase (ERK) have been demonstrated in zebrafish (Benman et al., 2022; Kainrath et al., 2017; Patel et al., 2019) and used to investigate ERK's influence on morphogenetic movements (Patel et al., 2019) and cell size/cycle regulation in the epidermis (Ramkumar et al., 2025). These compelling early studies showcase the novel research avenues that optogenetic technology can enable. However, to address gaps in our understanding of dynamic signal interpretation, optogenetic experiments introducing precise signaling inputs are ideal, but require in-depth knowledge of tool kinetics, responses to different light irradiances, and spatial activation properties. Therefore, a robustly characterized toolkit of optogenetic signaling activators with a unified design under identical conditions is valuable for use in developmental signaling investigations.

Toward these goals, here we present a comprehensive, direct comparison of an optogenetic toolkit to activate FGF, BMP, and Nodal signaling during zebrafish development. Our toolkit comprises a novel zebrafish-optimized FGF activator, a single-transcript Nodal activator, and an established BMP activator (Rogers et al., 2020). Here we show that light-mediated signaling activation by these tools *in vivo* is wavelength- and pathway-specific and leads to activation of known pathway target genes. We demonstrate that these tools activate signaling with distinct, rapid

on/off kinetics and that signaling activation strength depends on light irradiance. Finally, we demonstrate localized control of signaling with our novel FGF activator via spatially restricted light exposure. Together, our work provides a resource for zebrafish biologists in search of technology that enables straightforward, dynamic experimental activation of FGF, BMP, or Nodal signaling with high spatiotemporal control.

## RESULTS

### Optogenetic receptor kinase activator strategy

The optogenetic tools characterized here use the general activation strategy of light-mediated receptor kinase dimerization described in pioneering studies from 2014 (Chang et al., 2014; Crossman and Janovjak, 2022; Grusch et al., 2014; Kim et al., 2014). FGF, BMP, and Nodal pathways are all amenable to this strategy because they signal via a similar mechanism: Ligand binding to extracellular receptor domains initiates interactions between intracellular receptor kinases, leading to phosphorylation of an effector that translocates to the nucleus and regulates target gene expression together with other transcription factors (Derynck and Budi, 2019; Heldin and Moustakas, 2016; Ornitz and Itoh, 2015). To couple signaling activation to light rather than ligand exposure, intracellular receptor kinase domains can be fused to light-responsive dimerizing proteins. Light exposure can now activate signaling by inducing receptor kinase interactions. Because these fusions lack the receptor extracellular ligand binding domain, they are insensitive to extracellular ligand. The optogenetic tools characterized here are based on constructs developed by (Sako et al., 2016) and contain the flavin mononucleotide (FMN)-binding, blue light homodimerizing "light oxygen voltage-sensing" (LOV) domain AUREOCHROME variant from the algae *Vaucheria frigida* (VfAU1) (Takahashi et al., 2007; Toyooka et al., 2011) fused to zebrafish receptor kinase domains (Fig. 1). VfAU1 produced the most robust, reversible light-dependent activation compared to other LOV variants tested in cell culture in a pioneering study (Grusch et al., 2014). The constructs used here contain a myristoylation motif for membrane targeting and a C-terminal HA or FLAG tag for immuno-detection. We refer to these constructs as "bOpto" tools for **b**lue light **Opto**genetic signaling activators.

We first sought to create a zebrafish-optimized bOpto-FGF activator. Activation of FGF receptor kinases engages downstream signaling mediators, including SOS and MEK, culminating

in ERK phosphorylation (Ornitz and Itoh, 2015). Optogenetic ERK activators have been described in many systems (Choi et al., 2021; Csanaky et al., 2019; Dine et al., 2018; Grusch et al., 2014; Kim et al., 2014; Krishnamurthy et al., 2020; Pal et al., 2023; Rauschendorfer et al., 2021; Yadav et al., 2021). To our knowledge, three previous optogenetic ERK activators have been reported in zebrafish: 1) mFGFR1-MxCBD, a mouse FGF receptor intracellular domain fused to a cobalamin binding domain—a homodimer in the dark that dissociates with green light exposure (Kainrath et al., 2017), 2) BcLOV-$SOS_{cat}$, a fusion of the human RAS activator $SOS_{cat}$ (Toettcher et al., 2013) with the temperature-sensitive blue light homodimerizing domain BcLOV4 (Benman et al., 2022), 3) and $psMEK^{E203K}$, a constitutively active hamster MEK1 fused to 400/500 nm photoswitchable Dronpa monomers modified from (Zhou et al., 2017) by the addition of the cancer-associated activating E203K substitution (Patel et al., 2019; Ramkumar et al., 2025). These ERK activators feature human-, mouse-, or hamster-derived signaling components that may behave differently in different species. For example, in the process of creating optimized hamster-derived $psMEK^{E203K}$, preliminary experiments showed that a non-optimized psMEK tool (Zhou et al., 2017) had strong activity in *Drosophila* but weak activity in zebrafish (Patel et al., 2019). This could reflect low sensitivity of zebrafish to ectopic ERK signaling (Patel et al., 2019), or sub-optimal interactions between the hamster-derived kinase and zebrafish pathway components. In addition, BcLOV-$SOS_{cat}$ and $psMEK^{E203K}$ act downstream of the receptor kinase (Benman et al., 2022; Patel et al., 2019; Ramkumar et al., 2025), which is useful for interrogating the roles of a specific pathway branch but may not provide information about the entire FGF ligand-activated signaling cascade. Also, for practical reasons, we sought to develop a tool reversibly activated by blue light, rather than a tool that is active in the dark and inhibited by green light (Kainrath et al., 2017). Therefore, our objective was to design a bOpto tool that 1) uses a zebrafish-specific receptor kinase to recapitulate normal pathway interactions, 2) activates all pathway branches regulated by FGF ligand to mimic endogenous signaling, and 3) is activated by blue light (~450 nm), and reverts to the inactive state when returned to dark. In zebrafish, the five FGF receptors function largely redundantly, although phenotypes are uniquely observed when *fgfr1a* is knocked down in combination with any other receptor, suggesting that this receptor is a key FGF signaling mediator in the early embryo (Leerberg et al., 2019). We therefore fused everything downstream of the putative transmembrane domain from zebrafish Fgfr1a (zFgfr1a) to LOV to generate bOpto-FGF (Fig. 1A,A', Addgene #232639).

156 Next, we created a single-transcript version of a previously published optogenetic Nodal
157 activator. The original LOV-based bOpto-Nodal activator is composed of two constructs: VfAU1
158 fused to the serine/threonine kinase domains of the zebrafish type I receptor Acvr1ba and the type
159 II receptor Acvr2ba, respectively (Sako et al., 2016). To minimize potential for dark leakiness
160 (McNamara et al., 2025) and simplify handling, we created a single-transcript construct that codes
161 for both components. In "bOpto-2A-Nodal", a viral PTV-1 2A peptide sequence separates the two
162 coding sequences (Fig. 1C,C', Addgene #232640) (Kemmler et al., 2023; Ryan et al., 1991).
163 Ribosomes that encounter this 2A sequence during translation fail to form a peptide bond, leading
164 to release of the previously translated polypeptide; translation then continues after the 2A site
165 (Donnelly et al., 2001a; Donnelly et al., 2001b). We therefore expect bOpto-2A-Nodal to produce
166 two separate type I-LOV and type II-LOV proteins from a single mRNA. This approach has been
167 successful with other optogenetic systems (Humphreys et al., 2023; Krishnamurthy et al., 2020;
168 Ueda et al., 2022). In addition, we replaced the HA tag on the type II-LOV component with a
169 FLAG tag to facilitate immuno-detection of individual components (Fig. 1C).
170 The third tool in our kit is a previously established bOpto-BMP activator (Fig. 1B,B')
171 (Rogers et al., 2020; Saul, Rogers et al., 2023). This is a three-component system composed of
172 VfAU1 fused to the cytoplasmic domains of the zebrafish BMP receptors Bmpr1aa, Acvr1l, and
173 Bmpr2a. Previous work demonstrated robust BMP activation in zebrafish with minimal dark
174 leakiness (Rogers et al., 2020).
175 Together, bOpto-FGF, -BMP, and -2A-Nodal comprise the toolkit of zebrafish-specific
176 receptor kinase-based optogenetic signaling activators that we characterize herein.
177
178 **Wavelength dependent optogenetic activators of FGF, BMP, and Nodal signaling**
179 We first sought to determine whether bOpto tools activate their respective downstream
180 signaling pathways specifically in response to blue light exposure (455 nm). The VfAU1 domain
181 used here should homodimerize only in response to blue light (Mitra et al., 2012; Takahashi et al.,
182 2007; Toyooka et al., 2011). To empirically test the wavelength dependence of bOpto tools and
183 define "safe handling" conditions, we injected zebrafish embryos at the one-cell stage with mRNA
184 encoding *bOpto-FGF*, *bOpto-BMP*, or *bOpto-2A-Nodal*. mRNA amounts were titrated in earlier
185 experiments to optimize dynamic range (not shown). We then either maintained embryos in the
186 dark, exposed them to 455 nm light (50 W/m$^2$, Supp. Fig. 1A), or exposed them to 495+ nm light

187 (495-2200 nm, 18.51 W/m$^2$, Supp. Fig. 1B) from 2 hours post-fertilization (hpf) to 1 day post-
188 fertilization (dpf). Ectopic BMP signaling results in ventralization (V1-V4) at 1dpf (Kishimoto et
189 al., 1997; Nguyen et al., 1998; Schmid et al., 2000), whereas embryos experiencing strong ectopic
190 FGF or Nodal signaling have developmental defects and often lyse by 1 dpf (Feldman et al., 2002;
191 Fürthauer et al., 1997; Fürthauer et al., 2004; Rebagliati et al., 1998; Rogers et al., 2017). We used
192 these phenotypes as a convenient, rapid readout of ectopic signaling activation. At 1 dpf uninjected
193 controls appeared morphologically normal in all light conditions (Fig. 2A, Supp. Fig. 2),
194 suggesting minimal phototoxicity. Injected embryos maintained in the dark or exposed to 495+ nm
195 light were mostly morphologically indistinguishable from uninjected siblings. In contrast, injected
196 embryos exposed to 455 nm light had phenotypes consistent with strong ectopic activation of the
197 corresponding pathway. Our phenotype data indicates that exposure to 455 nm light robustly
198 activates bOpto tools, whereas we did not observe obvious ectopic signaling activation in the dark
199 or in response to 495+ nm light.

200 To directly assay activation of each pathway at an earlier developmental stage, we then
201 used hybridization chain reaction immunofluorescence (HCR-IF) (Schwarzkopf et al., 2021) to
202 assess phosphorylated effectors of FGF (ppERK), BMP (pSmad1), and Nodal (pSmad2) pathways.
203 We assessed signaling in *bOpto*-injected and uninjected embryos exposed to dark, 455 nm light,
204 or 495+ nm light for 30 minutes starting at early gastrulation (50% epiboly – shield) (Fig. 2B-D
205 and B'-D', Supp. Figs. 3 & 4). To account for non-uniform *bOpto* mRNA levels and distribution,
206 we include mRNA encoding *GFP* in our *bOpto* injection mixes (Lim et al., 2009). The mixture of
207 both *bOpto* and *GFP* mRNAs should be dispersed with the same relative distribution; as such,
208 GFP signal can be used as a proxy for bOpto tool distribution. Phosphorylated effector
209 fluorescence intensity measured by HCR-IF was normalized pixel-wise to GFP fluorescence
210 intensity to account for heterogeneity.

211 We did not notice differences in ppERK, pSmad1, or pSmad2 signal in uninjected embryos
212 across light conditions (Fig. 2B-D, Supp. Fig. 4), indicating that light exposure does not affect
213 these signaling pathways in this context. For all tools, there was a significant effect of wavelength
214 on normalized phosphorylated signaling effector levels ($p < 0.0001$) (Fig. 2B'-D', Supp. Figs. 3 &
215 4, Supplementary Materials). bOpto-FGF embryos exposed to 455 nm light showed a 2.9-fold
216 increase in normalized ppERK levels compared to dark ($p < 0.0001$), and a 3.5-fold increase when
217 compared to 495+ nm ($p < 0.0001$) (Fig. 2B'). In contrast, there were no differences between

218 bOpto-FGF embryos exposed to 495+ nm light versus dark ($p$ = 0.4099). Similarly, bOpto-2A-
219 Nodal embryos exposed to 455 nm light showed a 4.9-fold increase in normalized pSmad2 levels
220 compared to dark ($p < 0.0001$), and a 4.9-fold increase when compared to 495+ nm ($p < 0.0001$)
221 (Fig. 2D'). There were no differences between bOpto-2A-Nodal embryos exposed to 495+ nm
222 light versus dark ($p$ = 0.9997). Finally, bOpto-BMP embryos exposed to 455 nm light similarly
223 showed a 1.6-fold increase in normalized pSmad1 levels compared to dark ($p < 0.0001$), and a 1.5-
224 fold increase compared to 495+ nm ($p < 0.0001$). Levels in embryos exposed to 495+ nm were not
225 different from dark exposed embryos ($p$ = 0.9492) (Fig. 2C'). However, bOpto-BMP showed a
226 less clear increase in signaling in response to blue light compared to -FGF and -2A-Nodal, possibly
227 due to the presence of the endogenous ventral-to-dorsal pSmad1 signaling gradient (Rogers et al.,
228 2020; Tucker et al., 2008).
229 Together, our phenotype and HCR-IF results demonstrate robust bOpto-mediated signaling
230 activation with 455 nm light exposure and negligible activation when exposed to wavelengths
231 above 495nm (at 18.51 W/m$^2$) or when maintained in the dark. Based on these results, to safely
232 handle embryos expressing bOpto tools without inadvertent photoactivation of signaling
233 pathways, we use a light source with a peak wavelength well above 495 nm (~600 nm, Supp. Fig.
234 1C).
235
236 **bOpto tools activate expression of known pathway target genes**
237 Signaling activation leads to expression of pathway-specific target genes. To determine
238 whether bOpto-FGF, -BMP, and -2A-Nodal activate downstream target genes, we used
239 hybridization chain reaction fluorescence *in situ* hybridization (HCR-FISH) (Choi et al., 2018) to
240 assess expression of known pathway target genes. We exposed *bOpto*-injected and uninjected
241 embryos to dark or 455 nm light (50 W/m$^2$) for two hours starting before gastrulation (dome - 30%
242 epiboly stage), then fixed embryos and performed multiplexed HCR-FISH (Fig. 3). We chose a
243 two-hour exposure to allow enough time for ample transcript accumulation, and selected three
244 genes per pathway based on robust evidence implicating them as pathway targets: FGF = *spry4*,
245 *dusp6*, and *il17rd* (Fig. 3A) (Fürthauer et al., 2002; Fürthauer et al., 2001; Molina et al., 2007);
246 BMP = *sizzled*, *gata2a*, and *bambia* (Fig. 3B) (Greenfeld et al., 2021; Rogers et al., 2020); Nodal
247 = *lefty1*, *goosecoid*, and *noto* (Fig. 3C) (Bennett et al., 2007; Bisgrove et al., 1999). In all cases,
248 gene expression was similar in uninjected dark embryos, uninjected 455 nm light exposed

249 embryos, and injected dark embryos, suggesting negligible bOpto leakiness in the dark. In contrast,
250 455 nm light exposure activated gene expression in *bOpto*-expressing embryos. Together, our
251 results demonstrate robust optogenetic activation of known target genes by bOpto-FGF, -BMP, and
252 -2A-Nodal in zebrafish embryos, establishing that this suite of optogenetic activators provides
253 experimental access to major signaling pathways during zebrafish development.
254
255 **bOpto tools are pathway-specific**
256 Receptors can engage in cross-talk, in which pathway components canonically associated
257 with one signaling pathway are involved in transducing signaling from one or more additional
258 pathways (Derynck and Budi, 2019; Ramachandran et al., 2018). We therefore designed an
259 experiment to investigate whether cross-talk is associated with this suite of optogenetic signaling
260 activators. We injected zebrafish embryos at the one-cell stage with mRNA encoding *bOpto-FGF*,
261 *-BMP*, or *-2A-Nodal* and reared them in the dark until early gastrulation (50% epiboly – shield).
262 We then exposed half of the injected embryos, as well as uninjected control siblings, to 455 nm
263 light (50 $W/m^2$) for 30 minutes. To simultaneously detect phosphorylated signaling effectors from
264 all three pathways (FGF (ppERK), BMP (pSmad1), and Nodal (pSmad2)), we then performed
265 triple IF staining by modifying the dual IF protocol from (Soh et al., 2020).
266 In uninjected controls, signaling differences were not observed in dark compared to blue
267 light exposed embryos (Fig. 4), consistent with earlier HCR-IF experiments (Fig. 2). We also noted
268 minimal differences between uninjected embryos and injected embryos maintained in the dark,
269 again suggesting negligible leaky dark activation. Blue light-exposed bOpto-FGF embryos showed
270 strong ectopic ppERK activation, but no obvious ectopic pSmad1 or pSmad2 activity in any
271 condition (Fig. 4A). Similarly, blue light-exposed bOpto-BMP embryos had higher levels of
272 pSmad1 but no evident ectopic ppERK or pSmad2 activity in any condition (Fig. 4B). Embryos
273 expressing bOpto-2A-Nodal exposed to blue light had strong ectopic pSmad2 activation and
274 showed no changes in pSmad1 levels between conditions (Fig. 4C). We occasionally observed
275 embryos in bOpto-2A-Nodal experiments with possible ectopic ppERK activity (Supp. Fig. 5),
276 though this appears to be an IF or imaging artifact. Overall, bOpto-FGF, -BMP, and -2A-Nodal
277 generate robust pathway-specific optogenetic activation at the level of signaling in gastrulation
278 stage zebrafish.
279

280 **bOpto tools have rapid on/off kinetics**

281 Speed and reversibility are two benefits of optogenetic strategies (Rogers and Müller,
282 2020). These features are especially important in studies investigating how cells interpret signaling
283 (Farahani et al., 2021) to make fate decisions during early embryogenesis, where key patterning
284 events can occur in a matter of hours or even minutes (Huang et al., 2017; Sako et al., 2016). To
285 determine the on/off kinetics of bOpto-BMP, -FGF, and -2A-Nodal, we injected mRNA encoding
286 each respective tool together with *GFP* mRNA into zebrafish embryos at the one cell stage. At
287 early gastrulation stage (50% epiboly – shield) we exposed embryos to 455 nm light (50 $W/m^2$)
288 for 30 minutes, then removed light for a defined tool-dependent dark recovery period. We fixed
289 embryos at multiple time points throughout the exposure and recovery phases, together with time-
290 matched injected controls that were maintained in the dark the entire time. We then used HCR-IF
291 to quantify phosphorylated signaling effector levels corresponding to the stimulated pathway (Fig.
292 5). GFP signal was used to normalize *bOpto* mRNA amount and distribution. In addition,
293 normalized effector signal was background subtracted against dark controls (Supp. Figs. 6 & 7).
294 We observed clear signaling activation within the 30 min light exposure phase and a return to
295 baseline after light removal for all tools (Fig. 5A-C, A'-C').

296 First, to discern differences in "on" kinetics of the tools, we analyzed the light exposure
297 phase of the time course (Fig. 5A"-C"). Three-parameter logistic regressions were fit to the data.
298 From the model, three values were calculated approximating the time to reach a percentage of the
299 curve's upper asymptote: $tON_{20}$ predicting initial activation, $tON_{50}$ predicting half-maximum, and
300 $tON_{90}$ predicting saturation (Supplementary Materials). bOpto-FGF (curve fit $R^2 = 0.503$) had the
301 fastest on kinetics, reaching saturation within 2 minutes (Fig. 5A"). Because our assayed time
302 points were determined *a priori*, there was insufficient coverage between 0 and 2 min for confident
303 predictions of $tON_{20}$, $tON_{50}$, and $tON_{90}$. However, it is clear that initiation and saturation occur
304 between 0 and 2 min for bOpto-FGF. bOpto-BMP (curve fit $R^2 = 0.534$) had a $tON_{20}$ of 1.78 min
305 (CI: -4.97-8.53 min), a $tON_{50}$ of 6.36 min (CI: 1.35-11.37 min), and $tON_{90}$ of 13.62 min (CI: 0.75-
306 26.49 min) (Fig. 5B"). Of the three constructs, bOpto-2A-Nodal (curve fit $R^2 = 0.966$) had the
307 slowest on kinetics: it had a $tON_{20}$ of 16.12 min (CI: 12.25-19.99 min), a $tON_{50}$ of 19.78 min (CI:
308 16.13-23.43 min), and $tON_{90}$ of 25.59 min (CI: 14.04-37.14 min) (Fig. 5C"). Comparing initiation
309 times ($tON_{20}$), and assuming that this occurs for bOpto-FGF between 0-2 minutes, bOpto-2A-
310 Nodal is ~14 min slower than bOpto-FGF; bOpto-BMP and bOpto-FGF both likely initiate

activation before 2 minutes of light exposure. Comparing the tools' time to saturation ($tON_{90}$), again assuming that this occurs for bOpto-FGF within the first 2 minutes, bOpto-FGF is ~12 minutes faster than bOpto-BMP and ~24 minutes faster than bOpto-2A-Nodal. It also appears that the tools that clearly reach saturation prior to end of the 30 minute light exposure (bOpto-FGF and -BMP) maintain peak signaling levels until light removal.

Next, to discern differences in "off" kinetics of the tools, we analyzed the dark recovery phase of the time courses (Fig. 5A'''-C'''). In this phase, embryos that had been exposed to the 30 minute, 455 nm light pulse were incubated in the dark for an additional 55 (bOpto-FGF) or 90 (bOpto-BMP and -2A-Nodal) minutes. The same curve fitting approach that was used to determine the on kinetics was also used here to assess the off kinetics with a conceptual alteration: We calculated the time to a defined percentage *decrease* from the upper asymptote to reflect the progressive return to baseline (Supplementary Materials). For each tool we calculated $tOFF_{20}$ predicting time to initial deactivation, $tOFF_{50}$ predicting time to half-maximum, and $tOFF_{90}$ predicting approximate time to return to baseline. The off kinetics of bOpto-FGF (curve fit $R^2$ = 0.877) were the most rapid of the tested tools, with a $tOFF_{20}$ of 1.76 min (CI: -9.05-12.56 min), $tOFF_{50}$ of 5.30 min (CI: 2.72-7.88 min), and a $tOFF_{90}$ of 10.92 min (CI: -37.37-59.20 min). bOpto-BMP (curve fit $R^2$ = 0.667) was determined to have a $tOFF_{20}$ of 20.81 min (CI: 8.47-33.15 min), a $tOFF_{50}$ of 27.11 min (CI: 19.56-34.67 min), and a $tOFF_{90}$ of 37.10 min (CI: 20.99-53.21 min). Finally, bOpto-2A-Nodal (curve fit $R^2$ = 0.626) had the slowest off kinetics, with a $tOFF_{20}$ of 10.63 min (CI: -4.34-25.61 min), a $tOFF_{50}$ of 32.67 min (CI: 22.22-43.12 min), and a $tOFF_{90}$ of 67.60 min (CI: 33.56-101.63 min). Comparing the tools' time to initial deactivation ($tOFF_{20}$), bOpto-FGF began to decrease first, 9 min before bOpto-2A-Nodal and 19 min before bOpto-BMP. In contrast to bOpto-FGF and -2A-Nodal-induced signaling, which started to decrease relatively soon after light removal, bOpto-BMP-induced signaling was sustained into the dark period and then rapidly progressed towards baseline. Comparing time to return to baseline ($tOFF_{90}$), bOpto-2A-Nodal had the slowest return time, ~31 minutes slower than bOpto-BMP and ~57 minutes slower than bOpto-FGF.

Each tool's time to reach saturation in the light exposure phase ($tON_{90}$) was faster than its time to return to baseline after the light had been removed ($tOFF_{90}$). Additionally, the relative kinetics between the tools (e.g., bOpto-FGF fastest, bOpto-2A-Nodal slowest) was overall

consistent for both on and off kinetics. In summary, these data demonstrate that all tools in the bOpto toolkit activate signaling rapidly and reversibly.

**Optogenetic signaling activation is dependent on irradiance**

Another key advantage of optogenetic tools is the ability to adjust activation strength by modulating light irradiance (Rogers and Müller, 2020). This ability is particularly useful because different signaling levels can have distinct biological consequences (Johnson and Toettcher, 2019). To characterize the irradiance dependence of bOpto tools, we injected embryos with mRNA encoding *bOpto* constructs and *GFP* at the one-cell stage, then at early gastrulation (50% epiboly – shield) exposed embryos to 455 nm light (Supp. Fig. 1A) at eight different irradiances ranging from 0.02 to 50 W/m$^2$, changing roughly 3-fold between steps (Fig. 6A). Because bOpto-BMP and -2A-Nodal have slower times to saturation than bOpto-FGF (Fig. 5), we chose exposure durations of 5 minutes for bOpto-FGF and 25 minutes for bOpto-BMP and -2A-Nodal. We fixed embryos immediately after exposure and used HCR-IF to quantify the relevant phosphorylated signaling effector (Fig. 6), normalizing for mRNA level and distribution using GFP signal and background subtracting based on dark controls (Supp. Figs. 8 & 9).

For all three constructs, levels of phosphorylated signaling effectors increased with increasing light irradiance (Fig. 6). To characterize each tool's irradiance dependence, three-parameter logistic regressions were fit to the data. From the model, three values were calculated approximating the irradiance at which a percentage of the curve's upper asymptote is reached: $I_{20}$ predicting initial response, $I_{50}$ predicting half-maximum, and $I_{90}$ predicting saturation (Supplementary Materials). bOpto-FGF (curve fit $R^2 = 0.748$) was most sensitive to irradiance with an $I_{20}$ of 0.05 W/m$^2$ (CI: 0-0.11 W/m$^2$), an $I_{50}$ of 0.09 W/m$^2$ (CI: 0.03-0.15 W/m$^2$), and an $I_{90}$ of 0.15 W/m$^2$ (CI: 0.05-0.25 W/m$^2$). bOpto-BMP (curve fit $R^2 = 0.678$) had an $I_{20}$ of 0.16 W/m$^2$ (CI: -0.03-0.35 W/m$^2$), an $I_{50}$ of 0.35 W/m$^2$ (CI: 0.17-0.53 W/m$^2$), and an $I_{90}$ of 0.67 W/m$^2$ (CI: 0.26-1.08 W/m$^2$). bOpto-2A-Nodal (curve fit $R^2 = 0.578$) was the least sensitive to irradiance with an $I_{20}$ of 3.90 W/m$^2$ (CI: -0.27-8.06 W/m$^2$), an $I_{50}$ of 11.00 W/m$^2$ (CI: 5.54-16.45 W/m$^2$), and an $I_{90}$ of 22.25 W/m$^2$ (CI: 6.12-38.38 W/m$^2$). We speculate that the bOpto-2A-Nodal curve plateaus over the range of tested irradiances; however, additional coverage between 10-100 W/m$^2$ is needed to make a definite conclusion.

371 To directly compare the light sensitivity of these tools, we first need to account for the fact
372 that exposure durations differed by tool. We therefore converted the $I_{20}$ and $I_{90}$ to dosages ($J/m^2$)
373 by multiplying them by the duration of exposure (bOpto-FGF = 5 min; -BMP and -2A-Nodal = 25
374 min) and calculating fold changes between tools. Based on their dosage-adjusted $I_{20}$ values, bOpto-
375 FGF was activated at a 14-fold lower light dosage than -BMP and a 356-fold lower light dosage
376 than -2A-Nodal. Similarly, based on dosage-adjusted $I_{90}$ values, bOpto-FGF saturates at a 36-fold
377 lower light dosage than -BMP and a 1211-fold lower light dosage than -2A-Nodal. Together, our
378 results demonstrate tunable, light irradiance-dependent activation of FGF, BMP, and Nodal
379 signaling with this bOpto toolkit in zebrafish embryos.
380
381 **Spatially localized optogenetic signaling activation**
382 A valuable opportunity enabled by optogenetic tools is the ability to manipulate biological
383 processes with spatial precision (Rogers and Müller, 2020). Spatially resolved Nodal activation
384 was recently achieved in zebrafish using a CRY2-based optogenetic activator (McNamara et al.,
385 2025) and, at the level of gene expression, with the two-transcript LOV-based Nodal activator
386 (Sako et al., 2016). Localized signaling activation has also been demonstrated for bOpto-BMP in
387 zebrafish (Rogers et al., 2020). To our knowledge, FGF remains the only pathway activated by our
388 toolkit without evidence for local control via receptor kinase-based optogenetics in zebrafish.
389 We therefore co-injected *bOpto-FGF* and *nls-Kaede* mRNA at the one-cell stage. Kaede
390 is a green-to-red photoconvertible fluorescent protein that photoconverts at 405 nm (Ando et al.,
391 2002). *nls-Kaede* + *bOpto-FGF* expressing embryos were reared in the dark, then at early
392 gastrulation stage (shield and older) were irradiated with 445 nm light for 5 minutes using a laser
393 scanning confocal microscope within a 75 x 600 μm region of interest. During the first 3 minutes
394 of exposure, embryos simultaneously received 405 nm light in the same region of interest to
395 photoconvert Kaede-expressing cells. HCR-IF was then performed to detect the FGF signaling
396 effector ppERK. Ectopic ppERK signal overlapped the photoconverted Kaede signal,
397 demonstrating spatially localized FGF activation (Fig. 7, Supp. Fig. 10). In some embryos we
398 noted ERK phosphorylation in a dumbbell-like pattern around the edges of the illumination region.
399 We speculate that, due the sensitivity of bOpto-FGF, this may be caused by out-of-plane light from
400 our choice of illumination method—a confocal laser scanning microscope—that projects a cone-
401 like light volume onto the sample. Dumbbell-like activation was not observed in other illumination

402 paradigms that project non-angular pencil beam-like light (McNamara et al., 2025), and as such
403 might be reduced with different hardware. In summary, we demonstrate optogenetically activated
404 localized ERK phosphorylation in gastrulation stage zebrafish embryos using spatially restricted
405 light exposure.
406
407 **DISCUSSION**
408
409 **Rapid, spatially resolved optogenetic signaling activation in zebrafish**
410 Here we introduce a zebrafish-optimized optogenetic toolkit and provide the systematic in-
411 depth characterization necessary to use this suite of tools in a variety of experiments. The toolkit
412 is comprised of a novel FGF activator, a modified single-transcript Nodal activator, and a
413 previously established BMP activator. This head-to-head *in vivo* characterization enables direct
414 performance comparisons between the optogenetic signaling activators. We performed these
415 characterizations in a relevant developmental context—the gastrulating zebrafish—where all three
416 pathways are synergistically acting to pattern the embryonic axes. We show that bOpto tools enable
417 wavelength- and pathway-specific activation of FGF, BMP, and Nodal signaling (Figs. 2 & 4) and
418 target genes (Fig. 3) with the simple, easily controlled input of 455 nm light. Signaling can be
419 activated with rapid on/off kinetics (Fig. 5), ectopic signaling strength can be tuned by modulating
420 light irradiance (Fig. 6), and activation can be localized with spatially restricted illumination (Fig.
421 7). This optogenetic toolkit can therefore be a highly useful resource for investigations using
422 zebrafish as a model system.
423
424 **FGF, BMP, and Nodal pathway cross-talk**
425 We did not observe obvious, direct cross-activation of non-target pathways with bOpto
426 tools using triple ppERK, pSmad1, pSmad2 IF (Fig. 4). However, we only assessed FGF, BMP,
427 and Nodal signaling, and it is possible that other pathways could be inadvertently targeted by
428 bOpto tools. Here we assessed direct effects by focusing on a relatively short 30 minute light
429 exposure, during which signaling was ectopically activated for 20-30 minutes (Fig. 5). However,
430 with sufficiently long signaling durations, we would expect to observe inter-pathway effects
431 because FGF, BMP, and Nodal are known to engage in many downstream interactions. For
432 example, Nodal activates expression of the BMP inhibitor Chordin (Koshida et al., 2002; Kudoh

et al., 2004) and promotes transcription of FGF ligand (Bennett et al., 2007; Mathieu et al., 2004; van Boxtel et al., 2018). FGF inhibits BMP transcription (Fürthauer et al., 1997) and can block nuclear translocation of pSmad1 (Kretzschmar et al., 1997).

We occasionally observed possible ectopic activation of FGF signaling in bOpto-2A-Nodal experiments (Supp. Fig. 5), which appears to be an IF or imaging artifact. However, other possibilities include leaky Nodal activation leading to *fgf* transcription. Another confounding factor is the observation that ERK phosphorylation can be caused by mechanical damage even at early stages (Supp. Fig. 11). FGF/ERK signaling is known to be involved in injury and regeneration responses in zebrafish adults (De Simone et al., 2021; Owlarn et al., 2017; Poss et al., 2000; Whitehead et al., 2005), *Xenopus* embryos (Christen and Slack, 1999; LaBonne and Whitman, 1997; Li et al., 2013), and *Drosophila* embryos (Belacortu and Paricio, 2011). We do not believe this is a likely explanation, but we present this as an important consideration in the interpretation of ppERK IF data in early zebrafish embryos.

In summary, although bOpto tools are pathway-specific, optogenetic experiments involving long-term signaling activation may affect non-targeted pathways due to downstream pathway interactions, though this caveat is not exclusive to optogenetic strategies.

**bOpto tools have distinct on/off kinetics and irradiance sensitivities**

Our measurements revealed the temporal activation and deactivation properties of bOpto tools in zebrafish (Fig. 5, Supp. Figs. 6 & 7). All constructs in this toolkit have relatively fast on kinetics, in the order of minutes. Signaling activation is reversible, decreasing to baseline after light is removed. In addition, each tool takes longer to deactivate than to activate. Despite these similarities, the tools also have distinct kinetic properties. bOpto-FGF is the fastest signaling activator and bOpto-2A-Nodal is the slowest. bOpto-BMP on/off kinetics fall in between the other two tools, although we observed a unique reversion feature: Signaling was briefly sustained after light removal before rapidly returning to baseline. In contrast, there was a shorter lag between light removal and the decrease in ectopic signaling for bOpto-FGF and -2A-Nodal.

Overall, the signaling kinetics we measured for bOpto-BMP and bOpto-2A-Nodal in zebrafish are consistent with prior literature. As our zebrafish-optimized bOpto-FGF tool is novel, no literature comparisons are available. The kinetics we measured for bOpto-BMP are roughly consistent with those measured in the establishing study (Rogers et al., 2020). bOpto-2A-Nodal

464 signaling kinetics appeared to be similar to those measured for the two-component bOpto-Nodal
465 parent constructs (McNamara et al., 2025). bOpto-2A-Nodal on kinetics also appear roughly
466 similar to those measured for a recent CRY2-based Nodal activator, though the CRY2-based
467 construct may have faster off kinetics (Emig et al., 2024; McNamara et al., 2025). However,
468 differences in exposure conditions (e.g., wavelength, irradiance) complicate direct comparisons.

469 We observed similar trends with responses to irradiance (Fig. 6, Supp. Figs. 8 & 9).
470 Signaling activation by all tools increased as irradiance increased. bOpto-FGF activity was
471 initiated with very low light dosages, whereas activation from bOpto-2A-Nodal required much
472 higher light dosages, and bOpto-BMP was responsive to dosages between those that activated the
473 FGF and Nodal tools. Previous literature also reported light dosage-dependence for bOpto-BMP
474 (Rogers et al., 2020), the two-component bOpto-Nodal parent constructs, and the CRY2-based
475 Nodal activator (McNamara et al., 2025). The striking differences in light dosage sensitivity we
476 demonstrate here illustrate the importance of controlling and reporting light irradiances when using
477 the bOpto toolkit.

478 Although further molecular characterization would be required to explain the differences
479 in on/off kinetics and irradiance sensitivity between the bOpto tools, we speculate that several
480 factors may contribute. First, the phosphorylation kinetics of the receptor kinase domains may
481 differ, as well as the kinetics of phosphatases targeting pathway effectors. The kinase domain in
482 the FGF activator is a receptor tyrosine kinase, whereas the BMP and Nodal activators are
483 serine/threonine kinase-based. Receptor tyrosine kinase activity can be rapid (Farahani et al.,
484 2023), and zebrafish embryos treated with a MEK inhibitor show strong reduction in ERK
485 phosphorylation within just 10-20 minutes (Wilcockson et al., 2023). Another possible factor is
486 the number of components in each bOpto activator: bOpto-FGF is a one-component system,
487 whereas bOpto-2A-Nodal is composed of a type I and type II construct, and bOpto-BMP comprises
488 two type I and one type II constructs (Fig. 1). This may influence the fraction of productive
489 interactions formed upon light exposure. Finally, in the case of bOpto-2A-Nodal, the use of the 2A
490 peptide might contribute to its observed properties. bOpto-2A-Nodal consists of two Myr-tagged
491 constructs (Sako et al., 2016) separated by a 2A peptide that in principle produces two separate
492 membrane-localized proteins (Fig. 1C). However, the localization of these components has not
493 been directly tested. A previous report showed that a Myr-tagged construct downstream of a 2A
494 peptide failed to localize to the membrane in HEK293T cells (Hadpech et al., 2018), suggesting

that the type II-LOV component of bOpto-2A-Nodal may be cytoplasmic. If the type II-LOV construct is in fact located in the cytoplasm, activation kinetics could be delayed due to the larger search space of the cytoplasm vs. cell membrane. Conversely, other optogenetic receptor kinase-based activators in which one component is cytoplasmic have been demonstrated to robustly activate signaling with an improved signal to noise ratio (Krishnamurthy et al., 2020; McNamara et al., 2025). We observed minimal dark leakiness with bOpto-2A-Nodal. If the type II-LOV component of bOpto-2A-Nodal is cytoplasmic, this might explain the apparent improvement in dynamic range compared to previous observations from parent constructs (McNamara et al., 2025). To determine the subcellular localization of each component of bOpto-2A-Nodal, future studies could use immuno-detection of the HA tag on the type I-LOV component and the FLAG tag on the type II-LOV component.

Overall, our measurements demonstrate that signaling activation with the bOpto toolkit is rapid, reversible, and tunable in gastrulation-stage zebrafish. This characterization therefore provides a range of useful parameters that can be experimentally manipulated to generate signaling pulses with different durations and amplitudes.

**Strategies to optimize use of bOpto signaling activators**

Based on our work, we suggest four key practical recommendations for zebrafish researchers planning to incorporate bOpto signaling activators into their studies. First, it is crucial to inject the appropriate amount of functional mRNA to avoid weak or leaky activation. Controls should be included in every experiment as a quality assessment (Saul, Rogers et al., 2023). In addition, mRNA injections can lead to heterogeneous distribution of bOpto tools. Two strategies to mitigate these effects are 1) addition of GFP mRNA to injection mixes (as done here), or 2) fusing fluorescent proteins to bOpto tools. Fluorescent read outs can be used to identify embryos injected with appropriate mRNA amounts and to normalize for differences in distribution or levels. In experiments involving signaling quantification, we found that GFP normalization improved the signal to noise ratio and aided interpretability.

Second, we show that signaling was not detectibly activated by light over 495 nm (Fig. 2, Supp. Figs. 2, 3, & 4). Our 495+ nm light source (18.51 $W/m^2$) emitted light at a lower irradiance than our 455 nm source (50 $W/m^2$) (Supp. Fig. 1). However, >20 hours of 495+ nm light exposure at this relatively lower irradiance was insufficient to activate signaling based on phenotypes (Fig.

526 2A, Supp. Fig. 2). In contrast, as little as 0.15 W/m$^2$ 455 nm light for 5 minutes robustly activated
527 ectopic FGF signaling (Fig. 6, Supp. Fig. 9). We therefore recommend using light sources well
528 above 495 nm to safely handle embryos. This can be achieved with bespoke lightbulbs, or by
529 covering white light sources (e.g., microscope stages) with red filters.

530 Third, our characterization of on/off kinetics and irradiance responses indicate that bOpto
531 tools have distinct properties that should be considered when determining light exposure
532 conditions in experimental designs. For example, bOpto-FGF is several hundred-fold more
533 sensitive to light dosage and is also activated 10-20 minutes faster than bOpto-2A-Nodal (Figs. 5
534 & 6). Therefore, light exposure conditions that saturate signaling from bOpto-FGF may not even
535 initiate signaling from bOpto-2A-Nodal.

536 Fourth, a potential confounding factor in optogenetic experiments is light-induced
537 dysregulation of development. Circadian oscillations have been characterized in many organisms
538 including zebrafish (Dekens et al., 2003; Froland Steindal and Whitmore, 2019; Krylov et al.,
539 2021; Laranjeiro and Whitmore, 2014; Tamai et al., 2004; Whitmore et al., 2000; Ziv and Gothilf,
540 2006). Of the four circadian genes that we assayed in uninjected gastrulating zebrafish, three
541 showed significant light-mediated increases in gene expression by HCR-FISH (*cry2*, *per2*, *tefa*;
542 Supp. Fig. 12). It is unclear whether these changes in circadian gene expression affect
543 developmental signaling. However, we did not detect obvious impacts of 455 nm light exposure
544 on FGF, BMP, or Nodal signaling (Figs. 2B-D, B'-D', Fig. 4, Supp. Fig. 4), gene expression (Fig.
545 3), or morphology at 1 dpf (Fig. 2A, Supp. Fig. 2). We therefore speculate that the effects of light
546 exposure on circadian gene expression did not confound the interpretation of our results. However,
547 additional studies are needed to probe the effects of circadian gene responses in the context of
548 optogenetic experiments. We suggest that blue (e.g., 455 nm) light exposed uninjected controls
549 should be included in optogenetic experiments as a precaution.

550

551 **Prospects for optogenetic technology in developmental biology**

552 We foresee at least three major uses of bOpto tools to address outstanding questions. First,
553 to examine how cells decode these signaling features in a variety of contexts, our characterization
554 of bOpto on/off kinetics and light irradiance dependence can help researchers create bespoke
555 signaling inputs with desired amplitudes and durations. Second, it may be possible to multiplex
556 these tools and jointly manipulate multiple pathways—for example, to generate simultaneous

pulses of BMP and FGF signaling. This could facilitate studies examining how cells interpret combinatorial signaling, which appears to be a key patterning strategy (Briscoe and Small, 2015; Kicheva and Briscoe, 2023). Third, it will be valuable to use bOpto tools to impose tailored experimental signaling inputs in pathway loss-of-function mutants, as in (McNamara et al., 2025; Vopalensky et al., 2018). This could help define which features of signaling gradients are important for their patterning functions—e.g., slope, shape, dynamics—among other applications.

Finally, several technical advances would make optogenetic strategies even more accessible. A current challenge with bOpto tools is that they are introduced by mRNA injection, which is transient and can lead to inconsistent distribution. Transgenic lines expressing bOpto constructs would obviate these challenges. Converting the two-transcript bOpto-Nodal tool (Sako et al., 2016) into the single-transcript construct used here facilitates the generation of transgenics since only a single genomic insertion is necessary. In addition, we demonstrated local signaling activation via spatially restricted light exposure in gastrulation-stage zebrafish on the order of 10-100 μm. The resolution of optogenetic control is in principle limited only by the combination of focusing optics used in illumination hardware and the underlying biology of the optogenetic tool. With further experimental refinements it may be possible to activate with even finer spatial resolution. For example, cellular precision has been achieved in intact *Drosophila* embryos (Guglielmi et al., 2015; Izquierdo et al., 2018) and cell culture (Benedetti et al., 2018; Donahue et al., 2021). Finally, tools to manipulate additional pathways, inhibit signaling, and orthogonal tools activated by different wavelengths would unlock further experimental possibilities and provide more opportunities to explore unprecedented research avenues.

In summary, the suite of optogenetic FGF, BMP, and Nodal activators characterized here represents a powerful experimental platform for developmental biologists and beyond. This toolkit provides a path for exploring key developmental biology questions such as how signaling dynamics and spatial gradients regulate embryogenesis. We anticipate that this work will motivate a fruitful expansion of optogenetic technology in developmental biology research.

**Acknowledgements:** We thank the NIH zebrafish facility staff for maintaining our fish stocks and Matthew T. Monaghan for helping to test immunofluorescence staining strategies. We also thank Jeffrey A. Farrell and his lab, Pedro P. Rocha, Sarah E. Sheppard, Leah F. Rosin, Harry A. Burgess, Patrick Müller, and the NICHD Aquatics Affinity Group for helpful discussions.

**Competing interests:** No competing interests declared.

**Funding:** This work was supported by NIH Intramural funding ZIAHD009002-01 to KWR.

## MATERIALS & METHODS

### Zebrafish husbandry and mRNA injections

Zebrafish husbandry and research protocols were approved by the NICHD Animal Care and Use Committee in accordance with the Guide for the Care and Use of Laboratory Animals of the National Institutes of Health. The AB zebrafish wild type strain was used in all experiments. Embryos were incubated at 28 °C in embryo medium (reverse osmosis water, Instant Ocean Sea Salt (0.25 g/L), and $NaHCO_3$ (~0.06 g/L, depending on initial pH)). For injections, mRNA was synthesized from NotI-linearized pCS2+ plasmids (see Construct Sequences, Supplementary Materials) using SP6 mMessage mMachine kits (Invitrogen AM1340). 1 nl of injection mix containing mRNA and phenol red tracer was injected through the chorion at the one-cell stage. For experiments in Figs. 2, 5, and 6, and Supp. Figs. 6, 7, 8, and 9, 20 pg *GFP* mRNA (modified from (Lim et al., 2009)) was included in the same injection mix as *bOpto* mRNA. For all experiments, embryos were incubated at 28 °C immediately after injection. Between 1.5 - 2 hpf, healthy, fertilized embryos were transferred to 6-well dishes used in experiments, wrapped in aluminum foil to prevent light exposure (or immediately exposed to light for phenotyping at 1 dpf, see below and Fig. 2A and Supp. Fig. 2), and returned to 28 °C (Saul, Rogers et al., 2023). At 1 dpf, embryos were scored on Leica M80 stereoscopes. Representative phenotype images were acquired on Leica M80 stereoscopes with Flexacam C1 or C5 camera attachments (Fig. 2A and Supp. Fig. 2). The mRNA amounts injected for each optogenetic tool are listed below:

<u>bOpto-FGF</u> (Addgene #232639): 3.5 pg

<u>bOpto-BMP (combined in injection mix)</u>
bOpto-Bmpr1aa (Addgene # 207614): 23.4 pg

619 bOpto-Acvr1l (Addgene # 207615): 23.4 pg
620 bOpto-Bmpr2a (Addgene # 207616): 40.2 pg
621
622 bOpto-2A-Nodal (Addgene #232640): 10 pg
623
624 We have found that mRNA amounts are crucial: Inject too little, and optogenetic activation
625 is negligible, inject too much, and leaky ectopic dark activation will occur (Saul, Rogers et al.,
626 2023). In addition, we have anecdotally observed a decay in mRNA aliquot efficacy over time. We
627 therefore included phenotype controls in all experiments. From each experiment, a subset of
628 embryos was exposed to dark or 455 nm light starting at ~2 hpf and phenotypes were scored at 1
629 dpf. We only proceeded with experiments in which these controls demonstrated that the
630 appropriate amount of functional mRNA had been delivered. The following criteria were
631 implemented for inclusion:
632
633 *bOpto-FGF and -2A-Nodal experiments*
634 Proceed if at least 60% of injected, 455 nm-exposed embryos are severely deformed or lysed. In
635 addition to the criteria above, do not proceed if the dark injected condition exhibits more than 20%
636 of the following phenotypes: mild-severe deformity, lysed.
637
638 *bOpto-BMP experiments*
639 Proceed if, in the injected, 455 nm-exposed condition, 1) there are V2 or higher embryos present,
640 and 2) at least 60% of embryos show V1-V4 phenotypes (Kishimoto et al., 1997; Nguyen et al.,
641 1998; Schmid et al., 2000). In addition to the criteria above, do not proceed if the dark injected
642 condition exhibits more than 20% of the following phenotypes: V1-V4, mild-severe deformity,
643 lysed.
644
645 In addition, rare experiments in which uninjected embryos in both dark and light conditions had
646 high numbers of defects (over ~30%) were excluded.
647
648 **Safe embryo handling**

To protect embryos from light in “dark” conditions, 6-well dishes containing embryos were wrapped in aluminum foil. To handle light-sensitive embryos without incurring inadvertent photoactivation, in a windowless room with the door closed we used a ~600 nm red light source (Supp. Fig. 1C) (A19 9W Equivalent 60W, E26 Red LED Colored Light Bulb, UNILAMP, Cat. No. B0C7YZ4KSY). In experiments requiring manipulation or visualization of light-sensitive embryos on a dissecting scope, inadvertent photoconversion was prevented by covering the scope base/white light source with red gel filter paper (#E106, Rosco, Cat. No. 110084014805-E106). In experiments requiring fixation, embryos were fixed either under these red light conditions, or, for some light exposed embryos, in the LED incubator in which they were exposed to light.

**Whole embryo light exposure**

Embryos were exposed to 455 nm light using the “LED incubators” described previously (Saul, Rogers et al., 2023). To create a 495+ nm light source (18.51 W/m$^2$, Fig. 2, Supp. Fig. 2 & 12) a broadband (400 - 2200 nm) Quartz-Tungsten Halogen white light source (Thor Labs, Cat. No. QTH10/M) was used as the base emitter. A 2” x 2” square glass 495 nm long-pass filter (Thor Labs, Cat. No: FGL495S) was mounted to the source via a custom 3D printed adapter (design modified from: Thor Labs, Cat. No. SM2FH) to restrict emission wavelengths to 495+ nm. Emitted spectra from each light source was measured over the 200-1000 nm range using a compact spectrometer (Thor Labs, Cat. No. CCS200) with a cosine corrector (Thor Labs, Cat. No. CCSB1)

Desired irradiance was confirmed prior to all experiments. Power at the sample plane across the 350-1100 nm range was measured with a digital optical power meter (Thor Labs, Cat. No. PM100D) coupled to a microscope slide sensor head (Thor Labs, Cat. No. S170C). Measured power was converted to irradiance by dividing the power by the sensor head’s active detector area.

For the light irradiance experiments (Fig. 6), neutral density filters (Norman Pack of 3 Neutral Density (ND) 810551 Filters (5"), B & H Foto & Electronics Corp., Cat. No. NONDS5) were taped over the light output of the LED incubators (Saul, Rogers et al., 2023). Combinations of ND filters and adjustments to the LED power settings were tuned to achieve the desired irradiances.

**Spatial activation experiments**

679 For spatial activation experiments (Fig. 7, Supp. Fig 10), embryos were dechorionated
680 using pronase at the 1 cell stage before being injected with *bOpto-FGF* (3.5 pg) + *nlsKaede* (25
681 pg) mRNA. Post-dechorionation and injection, embryos were incubated at 28 °C on agarose-
682 coated petri dishes in the dark. Upon reaching 50% epiboly, embryos were carefully moved under
683 a safe handling light source to a fresh agarose-coated dish which had wells cast into the agarose to
684 maintain the embryos at a stable orientation (animal pole up) during light exposure (Zaucker et al.,
685 2021).
686 To restrict light to a small (75 x 600 µm) area within the embryo, an upright laser scanning
687 confocal microscope (Nikon AX-FN AXR-MP) was used as the illumination source. The light path
688 consisted of the emission from a combination of laser lines passing through a BS20/80
689 transmission/reflectance mirror and a Nikon CF145 W Apochromat 20x/1.0 Objective (Mat. No.
690 MRD77226) before reaching the sample plane. A 594 nm laser was used to position the sample in
691 the center of the field of view. A consistent focal plane for illumination was identified by finding
692 the apex of the animal pole and then moving the z-position 125 µm down towards the center of
693 the embryo. A 75 x 600 µm region of interest (ROI) was defined in the center of the 815 x 815 µm
694 field-of-view. Stimulation to the ROI was controlled using the AX and ND Stimulation modules
695 in Nikon Elements and was two consecutive blocks totaling a 5-minute exposure period: 1) 405
696 nm + 445 nm light scanning the ROI for 3 minutes and 2) 445 nm light only for 2 minutes.
697 Restricting 405 nm exposure to the first 3-minute block allowed sufficient Kaede photoconversion
698 while minimizing any potential phototoxicity. Laser power was set to 25% for 405 nm laser and
699 15% for 445 nm laser. Power measured at the sample plane was 5.6 µW for block 1 and 2.1 µW
700 for block 2. It took 1.02s to irradiate the 45,000 $\mu m^2$ ROI. Consequently, effective irradiance at the
701 sample plane over the stimulation period was 126.93 $W/m^2$ in block 1 and 47.60 $W/m^2$ in block 2.
702 The irradiance and dosage due to 445 nm only over the whole exposure period was 47.60 $W/m^2$
703 and 14280.00 $J/m^2$, respectively.
704 One embryo at a time was subjected to the exposure paradigm above. After exposure,
705 embryos were immediately fixed for downstream processing. Time-matched unexposed and
706 uninjected embryos were also fixed as controls.
707
708 **Triple pSmad1 + pSmad2 + ppERK immunofluorescence staining protocol**

709 To simultaneously detect phosphorylated effectors of FGF (ppERK), BMP (pSmad1), and
710 Nodal (pSmad2) signaling, we developed a triple immunofluorescence (IF) staining protocol based
711 on the pSmad1 + pSmad2 double IF protocol from (Soh et al., 2020). Note that primary antibodies
712 for pSmad1 and pSmad2 are both rabbit and detected with anti-rabbit secondaries; however, lower
713 pSmad2 epitope abundance and/or antibody affinity combined with amplification of the pSmad2
714 signal are thought to prevent significant crosstalk.

715 Embryos were fixed overnight at 4 °C in 4% formaldehyde in 1x PBS (phosphate buffered
716 saline). After washing 3x with 1x PBST (1x PBS + 0.1% Tween 20), embryos were manually
717 dechorionated using forceps. Embryos were washed 3x in MeOH and stored at -20 °C overnight
718 or longer. Embryos were then washed 4x with PBST, incubated at room temperature (RT) for 20
719 min in ice cold acetone, washed again with 4x with PBST, then blocked in 10% fetal bovine serum
720 (FBS) in 1x PBST at RT for ≥1 hour. Embryos were then incubated at 4 °C overnight in 1:5000
721 rabbit anti-pSmad2/3 primary antibody (Cell Signaling Technology #8828S) in 10% FBS. The
722 following day embryos were washed 5x in 1x PBST, re-blocked in 10% FBS for ≥1 hour at RT,
723 then incubated at 4 °C overnight in 1:500 goat anti-rabbit HRP secondary antibody (Jackson
724 ImmunoResearch Laboratories #111-035-003) in 10% FBS. Next, embryos were washed ≥5x with
725 1x PBST, incubated in Tyramide Signal Amplification (TSA) buffer (Akoya Biosciences
726 NEL744001KT) for ≥15 min at RT, and incubated in 1:75 fluorescein:amplification buffer dilution
727 for 45 min at RT. Embryos were then washed 4x with 1x PBST, and peroxidase was inactivated by
728 incubation with 1% $H_2O_2$ at RT for 25 min. After ≥5x washes with 1x PBST, embryos were
729 incubated in 10% FBS for ≥1 hr at RT and then in 1:5000 mouse anti-ppERK1/2 primary antibody
730 (Sigma-Aldrich #M8159) in 10% FBS at 4 °C overnight with rocking. Embryos were then washed
731 ≥5x in 1x PBST, incubated for ≥1 hr in 10% FBS at RT, then incubated at 4 °C overnight in 1:500
732 donkey anti-mouse HRP secondary antibody (Jackson ImmunoResearch Laboratories #715-035-
733 150) in 10% FBS. Following ≥5x PBST washes and a ≥15 min incubation in TSA amplification
734 buffer at RT, embryos were incubated for 45 min in a 1:75 Cy3:amplification buffer dilution. After
735 4x 1x PBST washes, embryos were washed 2x with MeOH, incubated at RT for ≥3 hours, re-
736 blocked in 10% FBS for ≥1 hour at RT, and then incubated in 1:100 rabbit anti-pSmad1/5/9
737 primary antibody (Cell Signaling Technology #13820S) at 4 °C overnight. The following day
738 embryos were washed ≥5x in 1x PBST, re-blocked in 10% FBS at RT for ≥1 hr, then incubated in
739 1:100 goat anti-rabbit Alexa647 secondary antibody (Invitrogen #A32733) and 1:5000 DAPI at 4

740 °C overnight. Embryos were washed ≥5x with 1x PBST, followed by 2x PBS washes, and imaged
741 within 1 month of staining completion.
742
743 **Hybridization Chain Reaction fluorescence *in situ* hybridization (HCR-FISH, mRNA**
744 **detection)**
745 Our hybridization chain reaction fluorescence *in situ* hybridization (HCR-FISH) protocol
746 is based on (Choi et al., 2018). Briefly, embryos were fixed in 4% formaldehyde at 4 °C overnight.
747 After the overnight fixation, the embryos were washed 3x with 1x PBST (1x PBS + 0.1% Tween
748 20) to stop fixation. Embryos were manually dechorionated in 1x PBST. The dechorionated
749 embryos were washed with 100% MeOH 3x, then stored overnight or longer at -20 °C.
750 Embryos were rehydrated briefly with 50% MeOH in PBST followed by 4x washes using
751 1x PBST. The residual PBST was carefully removed without disturbing the embryos. The embryos
752 were pre-hybridized at 37 °C with shaking at 300 rpm for 30 minutes in pre-warmed hybridization
753 buffer (Molecular Instruments). The HCR was multiplexed for simultaneous detection of three
754 different genes per pathway. Three different initiators (B1, B2, and B3) were used in combination
755 with three different pathway specific gene probes (Supp. Tables 11 & 12). The probe solution was
756 prepared by adding equal volumes of 1 uM probe solution to the pre-warmed hybridization buffer
757 (Molecular Instruments). Following pre-hybridization, embryos were incubated with the probe
758 hybridization solution at 37 °C for ≥12 hours with shaking at 300 rpm. After hybridization, excess
759 probe was removed by washing with probe wash buffer (Molecular Instruments) for 1 hour,
760 followed by washing the embryos with 5x SSCT (5x Saline-sodium citrate + 0.1% Tween 20) for
761 not more than 20 minutes.
762 Next, the pre-amplification was done by adding pre-warmed amplification buffer
763 (Molecular Instruments) and incubating embryos at room temperature for 30 minutes. The
764 amplification solution was prepared by snap cooling 30 pmol each of hairpin 1 and hairpin 2 for
765 three HCR amplifiers (B1-488, B2-546, and B3-647) in separate PCR tubes and combining them
766 with amplification buffer. The embryos were incubated with the amplification solution overnight
767 at room temperature with gentle rocking.
768 After amplification the embryos were washed briefly for 10 minutes with 5x SSCT and
769 then for a total of an hour. Embryos were then washed briefly with 1x PBST and stained with the
770 nuclear stain DAPI (1:5000) for 2 hours at room temperature. The embryos were then washed with

771 5x PBST at room temperature over 1 hour, then washed briefly 3x with 1x PBS. Embryos were
772 mounted using 1% LMP (Low melting point agarose) and imaged within two weeks after
773 processing.
774
775 **Hybridization Chain Reaction Immunofluorescence (HCR-IF, protein detection)**
776 Our hybridization chain reaction immunofluorescence (HCR-IF) protocol is based on
777 (Schwarzkopf et al., 2021). This protocol utilizes HCR-based signal amplification to detect
778 protein. In brief, the embryos were fixed with 4% formaldehyde in 1x PBS overnight at 4 °C. The
779 fixation was stopped by washing the embryos 4x with 1x PBST. Then embryos were washed with
780 100% MeOH 3x at room temperature to remove residual PBST. Embryos were permeabilized in
781 100% MeOH at -20 °C overnight or longer. The embryos were rehydrated by washing 4x using 1x
782 PBST. Then the embryos were blocked with antibody buffer (Molecular Instruments) for either ~4
783 hours at 4 °C or 1-4 hours at room temperature. The following primary antibodies were used: 1:100
784 rabbit anti-pSmad1/5/9 primary antibody (Cell Signaling Technology #13820S), 1:5000 rabbit
785 anti-pSmad2/3 primary antibody (Cell Signaling Technology #8828S) and 1:5000 mouse anti-
786 ppERK1/2 primary antibody (Sigma-Aldrich #M8159). Embryos were incubated in primary
787 antibody in antibody buffer overnight at 4 °C. The embryos were washed with 1x PBST for ≥2
788 hours with gentle rocking. Next, embryos were incubated in 1:1000 donkey-anti rabbit-B1
789 secondary antibody (Molecular Instruments) against rabbit anti-pSmad1, or 1:500 donkey-anti
790 rabbit-B1 secondary antibody (Molecular Instruments) against rabbit anti-pSmad2, or 1:500
791 donkey-anti mouse-B5 secondary antibody (Molecular Instruments) against mouse anti-ppERK
792 for 3 hours at room temperature. After incubation in secondary antibody, the embryos were washed
793 with 1x PBST for >30 minutes. After a brief rinse with 1x SSCT embryos were incubated in
794 amplification buffer (Molecular Instruments) for 30 minutes. The amplifier solution was prepared
795 by snap cooling hairpin 1 and hairpin 2 for corresponding HCR amplifiers (B1-647 or B5-647)
796 and combining them after snap cooling in amplification buffer. Embryos were incubated in HCR
797 amplification solution overnight at room temperature with gentle rocking, then washed with 5x
798 SSCT for 40 minutes and rinsed briefly with 1x PBST (For pSmad2 HCR-IF experiments in Figs.
799 5 and 6 and Supp. Figs. 6-9, amplification occurred at 4 °C. We found this led to better signal to
800 noise ratio for pSmad2). Embryos were then incubated in 1:5000 DAPI for 2.5 hours and washed

801 with 1x PBST for 1 hour, followed by a 1x PBS for 15 minutes and stored in PBS. Note that GFP
802 survives the MeOH incubation and HCR-IF protocol and was imaged directly.
803
804 **Confocal imaging**
805 Embryos that underwent HCR-FISH, HCR-IF, or triple immunofluorescence staining were
806 transferred to melted 1-1.2% low melting agarose (LMA) (in embryo medium) using a glass
807 pipette. Embryos were then immediately removed from the LMA, mounted on a plastic petri dish,
808 and oriented with the animal cap up using a stainless-steel needle. LMA was allowed to solidify
809 and 1x PBS was added to the petri dish before imaging the embryos.
810 IF, HCR-IF, and HCR-FISH-processed embryos were imaged using a Zeiss LSM 800
811 upright confocal laser scanning microscope. The light path consisted of the emission from one or
812 a combination of laser lines passing a W N-Achroplan 10x/0.3 objective before reaching the
813 sample plane. Reflected light was collected with 2 GaAsP-PMT and an Airyscan63 detectors. The
814 details of the laser lines and emission detection ranges used for all experiments are given in
815 Supplementary Table 1. Images were acquired with 0.7x zoom in bidirectional scanning mode with
816 16-bit depth, with a resolution of 512x512 pixels using ZEN microscopy software. For all
817 experiments, z-stacks were acquired with a 9 μm interval between slices, except for spatial
818 activation experiments in which a 10 μm interval was used. Remaining imaging settings (e.g., laser
819 power, gain, digital gain, line averaging, pixel dwell time) were consistently maintained for all
820 samples within a biological replicate (where there existed an internal dark control) for each
821 experiment and bOpto tool.
822
823 **Image Processing**
824 *Visualization Pipeline*
825 Triple IF images from pathway specificity experiments (Fig. 4 and Supp. Fig. 5) and HCR-
826 FISH gene expression experiments (Fig. 3) were processed using the same custom FIJI-based
827 pipeline (Supplementary Materials, Codes folder). In brief, for each sample, a maximum intensity
828 z-projection was generated, and lookup table for each acquired channel was adjusted to the defined
829 minimum and maximum values for that experiment.
830 HCR-IF images from wavelength dependence (Fig. 2), on/off kinetics (Fig. 5, Supp. Fig.
831 6), irradiance dependence (Fig. 6, Supp. Fig. 8), and spatial activation (Fig. 7, Supp. Fig. 10)

experiments, and HCR-FISH images from circadian experiments (Supp. Fig. 12) were processed using a custom MATLAB-based pipeline (Supplementary Materials, Codes folder). The user is prompted to supply lookup table bounds for visualization; this was kept consistent within each experiment and pathway. Maximum intensity z-projections were then generated for each sample and channel. Additionally, the user is prompted to identify a threshold for nuclear segmentation based on the DAPI or Kaede Green channels. Afterwards, a 3D mask defining the nuclear region is generated (hereby termed "DAPI region") and applied voxelwise to the effector signal channel image volume. A "nuclear" maximum intensity projection is then generated.

*Quantification Pipeline*

For all HCR-IF experiments needing downstream effector signal normalization and quantification (wavelength dependence (Fig. 2, Supp. Figs. 3 & 4), on/off kinetics (Fig. 5, Supp. Figs. 6 & 7), irradiance dependence (Fig. 6, Supp. Figs. 8 & 9)), the MATLAB-pipeline then prompts the user to specify a threshold for the GFP channel. Like nuclear thresholding, a 3D mask defining the "GFP region" is generated. The intersection between the DAPI and GFP regions was also calculated as the "DAPI+GFP region". The effector signal channel image volume is divided voxelwise by the GFP channel image volume, creating a "normalized signal" data volume. The following median values are then calculated for the imaged volume: 1) raw effector signal within the DAPI region, 2) GFP-normalized effector signal within the DAPI region, 3) raw effector signal within the GFP region, 4) GFP-normalized effector signal within the GFP region, 5) raw effector signal within the DAPI+GFP region, and 6) GFP-normalized effector signal within the DAPI+GFP region. Maximum z-projections of masks are exported for quality control assessment. Nuclear and GFP thresholds were kept consistent for all samples within a biological replicate (where there existed an internal dark control) for each experiment and bOpto tool. For FGF and BMP, the median GFP-normalized effector signal within the GFP region was used in all downstream analyses. As Nodal effector, pSmad2, is largely nuclear the median GFP-normalized effector signal within the DAPI+GFP region was used.

*Quality Control*

Output data was then assessed for quality by 1-2 authors before additional processing. If any of the following criteria were met through screening maximum intensity projections, that

sample was thrown out: 1) damage was apparent in the DAPI channel spanning 1/3 of the embryo, 2) any part of the embryo was out of frame, 3) a portion of an errant second embryo was in frame, 4) the embryo was mounted on an angle (>40 degrees off axis), 5) z-stack does not encompass entire embryo. If the following criteria was met through screening maximum intensity projections, that entire exposure group within the biological replicate was removed: saturation-induced "streaking" present in any one channel. If the following criteria was met through screening masks, that sample was removed: <5% of the embryo was covered by the appropriate GFP mask, indicating a sample did not receive enough mRNA for analysis.

Any embryo imaged that passed all inclusion criteria was defined as a technical replicate within an exposure condition and biological replicate for the appropriate experiment. Sufficient "trials" were run for each experiment such that 3 biological replicates were acquired for all assayed conditions within each experiment. GFP-normalized signal for all technical replicates within an exposure condition, biological replicate, and bOpto tool were averaged together and processed as follows for the corresponding experiments:

*Wavelength Dependence*

For each bOpto tool, the mean GFP-normalized signal for all samples within each wavelength (Dark, 495+ nm, 455nm) and biological replicate was fit by a linear mixed-effects model (Fixed Effect: Wavelength, Random Effect: Biological Replicate; Personality: Standard Least Squares, Method: REML). Predicted least square means and standard error were calculated for each wavelength. Where warranted by a significant ($p < 0.05$) fixed effect, *post hoc* comparisons were performed between all exposure combinations and corrected for multiple comparisons with Tukey's HSD method where $p < 0.05$ was considered to be statistically significant (Supp. Tables 2-4).

*On/Off Kinetics*

For each bOpto tool, the mean GFP-normalized signal for all 455 nm exposed samples within each time point (FGF: 0, 2, 8, 15, 22, 30, 35, 50, 60, 70, and 85 min; BMP/Nodal: 0, 2, 8, 18, 30, 35, 50, 60, 70, 85, and 120 min) and biological replicate was subtracted by its time-matched dark control. The dark-subtracted, normalized data was then analyzed by a one-way ANOVA with a fixed effect of time. Where warranted by a significant ($p < 0.05$) fixed effect, *post hoc*

comparisons were performed between each time point and time = 0 min with Dunnett's method for multiple comparison correction where $p < 0.05$ was considered to be statistically significant (Supp. Tables 6-7).

Next, models were fit to the dark-subtracted, GFP-normalized dataset to calculate estimates for on and off kinetic parameters. One model was generated for the "On" portion of the data (time <= 30) and a second model was fit to the "Off" portion of the data (time >= 30). We chose to fit a three-parameter logistic regression to each data subset. The equation for this model is defined as:

$$y = \frac{c}{1 + e^{(-a(x-b))}} \quad \text{(Eq.1)}$$

where y is the dark-subtracted normalized signal [AU], x is time [min], a is the growth rate [$min^{-1}$], b is the inflection point [min], and c is the upper asymptote [AU].

This curve fit has two underlying assumptions: 1) the general behavior of the bOpto tools will follow a tri-phasic lag-growth/decay-plateau behavior, and 2) the lower asymptote will be 0 (i.e., for "ON" the dark subtracted, normalized signal begins at zero; for "OFF" the dark subtracted, normalized signal will eventually return to zero at some point in time). $R^2$ was reported as the goodness of fit for each model. The predicted value of each factor (a, b, c) and its corresponding 95% confidence interval is also reported (Supp. Tables 8-9).

Additionally for the model fitting the "on" data, we used the predicted equation to solve for time at various points along the curve to more easily describe the activation kinetics. (Supplementary Materials) We took the value for the upper asymptote, c, and calculated three different percentages (20%, 50%, and 90%) of that value. We then used the curve fit equation to predict the time it takes from the start to reach those values. These conceptually represent: $tON_{20}$ predicting initial activation, $tON_{50}$ predicting half-maximum, and $tON_{90}$ predicting saturation. Additionally, for the model fitting the "off" data, we performed an analogous analysis with one modification: we calculated the time from light removal to reach three different percentage *decreases* of the upper asymptote (20%, 50%, and 90% decreases). These conceptually represent: $tOFF_{20}$ predicted time to initial deactivation, $tOFF_{50}$ predicted time to half-maximum, and $tOFF_{90}$ predicted approximate time to return to baseline. The predicted value of each tON and tOFF factor and its corresponding 95% confidence interval was reported in (Supp. Tables 8-9).

*Irradiance Dependence*

For each bOpto tool, the mean GFP-normalized signal for all samples within each irradiance (0, 0.02, 0.05, 0.15, 0.46, 1.39, 4.17, 12.50, 50.00 $W/m^2$) and biological replicate was subtracted by its round-matched dark control (Supp. Table 10). Data were fit with the same three-parameter logistic regression model used in the on/off kinetics experiments. (Eq. 1) The predicted value of each factor (a, b, c) and its corresponding 95% confidence interval was reported. From the model, three values were calculated approximating the irradiance at which a percentage (20%, 50%, and 90%) of the curve's upper asymptote is reached: $I_{20}$ predicting initial response, $I_{50}$ predicting half-maximum, and $I_{90}$ predicting saturation. The predicted value of each factor and its corresponding 95% confidence interval was reported in (Supp. Table 10).

**References:**


**Ando, R., Hama, H., Yamamoto-Hino, M., Mizuno, H. and Miyawaki, A.** (2002). An optical marker based on the UV-induced green-to-red photoconversion of a fluorescent protein. *Proc Natl Acad Sci U S A* **99**, 12651-12656.

**Belacortu, Y. and Paricio, N.** (2011). Drosophila as a model of wound healing and tissue regeneration in vertebrates. *Dev Dyn* **240**, 2379-2404.

**Benedetti, L., Barentine, A. E. S., Messa, M., Wheeler, H., Bewersdorf, J. and De Camilli, P.** (2018). Light-activated protein interaction with high spatial subcellular confinement. *Proc Natl Acad Sci U S A* **115**, E2238-E2245.

**Benman, W., Berlew, E. E., Deng, H., Parker, C., Kuznetsov, I. A., Lim, B., Siekmann, A. F., Chow, B. Y. and Bugaj, L. J.** (2022). Temperature-responsive optogenetic probes of cell signaling. *Nat Chem Biol* **18**, 152-160.

**Bennett, J. T., Joubin, K., Cheng, S., Aanstad, P., Herwig, R., Clark, M., Lehrach, H. and Schier, A. F.** (2007). Nodal signaling activates differentiation genes during zebrafish gastrulation. *Dev Biol* **304**, 525-540.

**Bisgrove, B. W., Essner, J. J. and Yost, H. J.** (1999). Regulation of midline development by antagonism of lefty and nodal signaling. *Development* **126**, 3253-3262.

**Bosman, S. L. and Sonnen, K. F.** (2022). Signaling oscillations in embryonic development. *Curr Top Dev Biol* **149**, 341-372.

**Briscoe, J. and Small, S.** (2015). Morphogen rules: design principles of gradient-mediated embryo patterning. *Development* **142**, 3996-4009.

957 **Buckley, C. E.** (2019). Optogenetic Control of Subcellular Protein Location and Signaling in
958 Vertebrate Embryos. *Methods Mol Biol* **1920**, 143-162.

959 **Buckley, C. E., Moore, R. E., Reade, A., Goldberg, A. R., Weiner, O. D. and Clarke, J. D. W.**
960 (2016). Reversible optogenetic control of subcellular protein localization in a live vertebrate
961 embryo. *Dev Cell* **36**, 117-126.

962 **Čapek, D., Smutny, M., Tichy, A. M., Morri, M., Janovjak, H. and Heisenberg, C. P.** (2019).
963 Light-activated Frizzled7 reveals a permissive role of non-canonical wnt signaling in
964 mesendoderm cell migration. *Elife* **8**, e42093.

965 **Chang, K. Y., Woo, D., Jung, H., Lee, S., Kim, S., Won, J., Kyung, T., Park, H., Kim, N.,**
966 **Yang, H. W., et al.** (2014). Light-inducible receptor tyrosine kinases that regulate neurotrophin
967 signalling. *Nat Commun* **5**, 4057.

968 **Choi, H. M. T., Schwarzkopf, M., Fornace, M. E., Acharya, A., Artavanis, G., Stegmaier, J.,**
969 **Cunha, A. and Pierce, N. A.** (2018). Third-generation in situ hybridization chain reaction:
970 multiplexed, quantitative, sensitive, versatile, robust. *Development* **145**.

971 **Choi, I. Y., Lim, H., Huynh, A., Schofield, J., Cho, H. J., Lee, H., Andersen, P., Shin, J. H.,**
972 **Heo, W. D., Hyun, S. H., et al.** (2021). Novel culture system via wirelessly controllable optical
973 stimulation of the FGF signaling pathway for human and pig pluripotency. *Biomaterials* **269**,
974 120222.

975 **Christen, B. and Slack, J. M.** (1999). Spatial response to fibroblast growth factor signalling in
976 Xenopus embryos. *Development* **126**, 119-125.

977 **Crossman, S. H. and Janovjak, H.** (2022). Light-activated receptor tyrosine kinases: Designs
978 and applications. *Curr Opin Pharmacol* **63**, 102197.

979 **Csanaky, K., Hess, M. W. and Klimaschewski, L.** (2019). Membrane-Associated, Not
980 Cytoplasmic or Nuclear, FGFR1 Induces Neuronal Differentiation. *Cells* **8**.

981 **De Simone, A., Evanitsky, M. N., Hayden, L., Cox, B. D., Wang, J., Tornini, V. A., Ou, J.,**
982 **Chao, A., Poss, K. D. and Di Talia, S.** (2021). Control of osteoblast regeneration by a train of
983 Erk activity waves. *Nature*.

984 **Dekens, M. P., Santoriello, C., Vallone, D., Grassi, G., Whitmore, D. and Foulkes, N. S.**
985 (2003). Light regulates the cell cycle in zebrafish. *Curr Biol* **13**, 2051-2057.

986 **Derynck, R. and Budi, E. H.** (2019). Specificity, versatility, and control of TGF-beta family
987 signaling. *Sci Signal* **12**.

988 **Dine, E., Gil, A. A., Uribe, G., Brangwynne, C. P. and Toettcher, J. E.** (2018). Protein phase
989 separation provides long-term memory of transient spatial stimuli. *Cell Syst* **6**, 655-663 e655.

**Donahue, C. E. T., Siroky, M. D. and White, K. A.** (2021). An Optogenetic Tool to Raise Intracellular pH in Single Cells and Drive Localized Membrane Dynamics. *J Am Chem Soc* **143**, 18877-18887.

**Donnelly, M. L. L., Hughes, L. E., Luke, G., Mendoza, H., Ten Dam, E., Gani, D. and Ryan, M. D.** (2001a). The 'cleavage' activities of foot-and-mouth disease virus 2A site-directed mutants and naturally occurring '2A-like' sequences. *J Gen Virol* **82**, 1027-1041.

**Donnelly, M. L. L., Luke, G., Mehrotra, A., Li, X., Hughes, L. E., Gani, D. and Ryan, M. D.** (2001b). Analysis of the aphthovirus 2A/2B polyprotein 'cleavage' mechanism indicates not a proteolytic reaction, but a novel translational effect: a putative ribosomal 'skip'. *J Gen Virol* **82**, 1013-1025.

**Emig, A. A., Hansen, M., Grimm, S., Coarfa, C., Lord, N. D. and Williams, M. K.** (2024). Temporal dynamics of BMP/Nodal ratio drive tissue-specific gastrulation morphogenesis. *Development*.

**Farahani, P. E., Reed, E. H., Underhill, E. J., Aoki, K. and Toettcher, J. E.** (2021). Signaling, Deconstructed: Using Optogenetics to Dissect and Direct Information Flow in Biological Systems. *Annu Rev Biomed Eng* **23**, 61-87.

**Farahani, P. E., Yang, X., Mesev, E. V., Fomby, K. A., Brumbaugh-Reed, E. H., Bashor, C. J., Nelson, C. M. and Toettcher, J. E.** (2023). pYtags enable spatiotemporal measurements of receptor tyrosine kinase signaling in living cells. *Elife* **12**.

**Feldman, B., Concha, M. L., Saude, L., Parsons, M. J., Adams, R. J., Wilson, S. W. and Stemple, D. L.** (2002). Lefty antagonism of squint is essential for normal gastrulation. *Current Biology* **12**, 2129-2135.

**Froland Steindal, I. A. and Whitmore, D.** (2019). Circadian Clocks in Fish-What Have We Learned so far? *Biology (Basel)* **8**.

**Fürthauer, M., Lin, W., Ang, S. L., Thisse, B. and Thisse, C.** (2002). Sef is a feedback-induced antagonist of Ras/MAPK-mediated FGF signalling. *Nat Cell Biol* **4**, 170-174.

**Fürthauer, M., Reifers, F., Brand, M., Thisse, B. and Thisse, C.** (2001). sprouty4 acts in vivo as a feedback-induced antagonist of FGF signaling in zebrafish. *Development* **128**, 2175-2186.

**Fürthauer, M., Thisse, C. and Thisse, B.** (1997). A role for FGF-8 in the dorsoventral patterning of the zebrafish gastrula. *Development* **124**, 4253-4264.

**Fürthauer, M., Van Celst, J., Thisse, C. and Thisse, B.** (2004). Fgf signalling controls the dorsoventral patterning of the zebrafish embryo. *Development* **131**, 2853-2864.

**Greenfeld, H., Lin, J. and Mullins, M. C.** (2021). The BMP signaling gradient is interpreted through concentration thresholds in dorsal-ventral axial patterning. *PLoS Biol* **19**, e3001059.

1024 **Grusch, M., Schelch, K., Riedler, R., Reichhart, E., Differ, C., Berger, W., Ingles-Prieto, A.**
1025 **and Janovjak, H.** (2014). Spatio-temporally precise activation of engineered receptor tyrosine
1026 kinases by light. *EMBO J* **33**, 1713-1726.

1027 **Guglielmi, G., Barry, J. D., Huber, W. and De Renzis, S.** (2015). An optogenetic method to
1028 modulate cell contractility during tissue morphogenesis. *Dev Cell* **35**, 646-660.

1029 **Guillotin, B. and Birnbaum, K. D.** (2020). Just passing through: The auxin gradient of the root
1030 meristem. *Curr Top Dev Biol* **137**, 433-454.

1031 **Hadpech, S., Jinathep, W., Saoin, S., Thongkum, W., Chupradit, K., Yasamut, U.,**
1032 **Moonmuang, S. and Tayapiwatana, C.** (2018). Impairment of a membrane-targeting protein
1033 translated from a downstream gene of a "self-cleaving" T2A peptide conjunction. *Protein Expr*
1034 *Purif* **150**, 17-25.

1035 **Heldin, C. H. and Moustakas, A.** (2016). Signaling Receptors for TGF-beta Family Members.
1036 *Cold Spring Harb Perspect Biol* **8**.

1037 **Hill, C. S.** (2022). Establishment and interpretation of NODAL and BMP signaling gradients in
1038 early vertebrate development. *Curr Top Dev Biol* **149**, 311-340.

1039 **Huang, A., Amourda, C., Zhang, S., Tolwinski, N. S. and Saunders, T. E.** (2017). Decoding
1040 temporal interpretation of the morphogen Bicoid in the early Drosophila embryo. *Elife* **6**,
1041 e26258.

1042 **Humphreys, P. A., Woods, S., Smith, C. A., Bates, N., Cain, S. A., Lucas, R. and Kimber, S.**
1043 **J.** (2020). Optogenetic Control of the BMP Signaling Pathway. *ACS Synth Biol*.

1044 **Humphreys, P. E. A., Woods, S., Bates, N., Rooney, K. M., Mancini, F. E., Barclay, C.,**
1045 **O'Flaherty, J., Martial, F. P., Domingos, M. A. N. and Kimber, S. J.** (2023). Optogenetic
1046 manipulation of BMP signaling to drive chondrogenic differentiation of hPSCs. *Cell Rep* **42**,
1047 113502.

1048 **Izquierdo, E., Quinkler, T. and De Renzis, S.** (2018). Guided morphogenesis through
1049 optogenetic activation of Rho signalling during early Drosophila embryogenesis. *Nat Commun* **9**,
1050 2366.

1051 **Johnson, H. E. and Toettcher, J. E.** (2018). Illuminating developmental biology with cellular
1052 optogenetics. *Curr Opin Biotechnol* **52**, 42-48.

1053 **Johnson, H. E. and Toettcher, J. E.** (2019). Signaling dynamics control cell fate in the early
1054 *Drosophila* embryo. *Developmental Cell* **48**, 361-370.e363.

1055 **Jones, W. D. and Mullins, M. C.** (2022). Cell signaling pathways controlling an axis organizing
1056 center in the zebrafish. *Curr Top Dev Biol* **150**, 149-209.

1057 **Kainrath, S., Stadler, M., Reichhart, E., Distel, M. and Janovjak, H.** (2017). Green-light-
1058 induced inactivation of receptor signaling using cobalamin-binding domains. *Angew Chem Int*
1059 *Ed Engl* **56**, 4608-4611.

1060 **Kemmler, C. L., Moran, H. R., Murray, B. F., Scoresby, A., Klem, J. R., Eckert, R. L.,**
1061 **Lepovsky, E., Bertho, S., Nieuwenhuize, S., Burger, S., et al.** (2023). Next-generation
1062 plasmids for transgenesis in zebrafish and beyond. *Development* **150**.

1063 **Kicheva, A. and Briscoe, J.** (2023). Control of Tissue Development by Morphogens. *Annu Rev*
1064 *Cell Dev Biol* **39**, 91-121.

1065 **Kim, N., Kim, J. M., Lee, M., Kim, C. Y., Chang, K. Y. and Heo, W. D.** (2014).
1066 Spatiotemporal control of fibroblast growth factor receptor signals by blue light. *Chem Biol* **21**,
1067 903-912.

1068 **Kishimoto, Y., Lee, K. H., Zon, L., Hammerschmidt, M. and Schulte-Merker, S.** (1997). The
1069 molecular nature of zebrafish swirl: BMP2 function is essential during early dorsoventral
1070 patterning. *Development* **124**, 4457-4466.

1071 **Kolar, K., Knobloch, C., Stork, H., Znidaric, M. and Weber, W.** (2018). OptoBase: A web
1072 platform for molecular optogenetics. *ACS Synth Biol* **7**, 1825-1828.

1073 **Koshida, S., Shinya, M., Nikaido, M., Ueno, N., Schulte-Merker, S., Kuroiwa, A. and**
1074 **Takeda, H.** (2002). Inhibition of BMP activity by the FGF signal promotes posterior neural
1075 development in zebrafish. *Dev Biol* **244**, 9-20.

1076 **Kretzschmar, M., Doody, J. and Massague, J.** (1997). Opposing BMP and EGF signalling
1077 pathways converge on the TGF-beta family mediator Smad1. *Nature* **389**, 618-622.

1078 **Krishnamurthy, V. V., Fu, J., Oh, T. J., Khamo, J., Yang, J. and Zhang, K.** (2020). A
1079 Generalizable Optogenetic Strategy to Regulate Receptor Tyrosine Kinases during Vertebrate
1080 Embryonic Development. *J Mol Biol* **432**, 3149-3158.

1081 **Krylov, V. V., Izvekov, E. I., Pavlova, V. V., Pankova, N. A. and Osipova, E. A.** (2021).
1082 Circadian rhythms in zebrafish (Danio rerio) behaviour and the sources of their variability. *Biol*
1083 *Rev Camb Philos Soc* **96**, 785-797.

1084 **Kudoh, T., Concha, M. L., Houart, C., Dawid, I. B. and Wilson, S. W.** (2004). Combinatorial
1085 Fgf and Bmp signalling patterns the gastrula ectoderm into prospective neural and epidermal
1086 domains. *Development* **131**, 3581-3592.

1087 **LaBelle, J., Ramos-Martinez, A., Shen, K., Motta-Mena, L. B., Gardner, K. H., Materna, S.**
1088 **C. and Woo, S.** (2021). TAEL 2.0: An Improved Optogenetic Expression System for Zebrafish.
1089 *Zebrafish* **18**, 20-28.

1090 **LaBonne, C. and Whitman, M.** (1997). Localization of MAP kinase activity in early Xenopus
1091 embryos: implications for endogenous FGF signaling. *Dev Biol* **183**, 9-20.

1092 **Laranjeiro, R. and Whitmore, D.** (2014). Transcription factors involved in retinogenesis are
1093 co-opted by the circadian clock following photoreceptor differentiation. *Development* **141**, 2644-
1094 2656.

1095 **Leerberg, D. M., Hopton, R. E. and Draper, B. W.** (2019). Fibroblast Growth Factor Receptors
1096 Function Redundantly During Zebrafish Embryonic Development. *Genetics* **212**, 1301-1319.

1097 **Li, J., Zhang, S., Soto, X., Woolner, S. and Amaya, E.** (2013). ERK and phosphoinositide 3-
1098 kinase temporally coordinate different modes of actin-based motility during embryonic wound
1099 healing. *J Cell Sci* **126**, 5005-5017.

1100 **Liberali, P. and Schier, A. F.** (2024). The evolution of developmental biology through
1101 conceptual and technological revolutions. *Cell*.

1102 **Lim, S. M., Pereira, L., Wong, M. S., Hirst, C. E., Van Vranken, B. E., Pick, M., Trounson,**
1103 **A., Elefanty, A. G. and Stanley, E. G.** (2009). Enforced expression of Mixl1 during mouse ES
1104 cell differentiation suppresses hematopoietic mesoderm and promotes endoderm formation. *Stem*
1105 *Cells* **27**, 363-374.

1106 **Mathieu, J., Griffin, K., Herbomel, P., Dickmeis, T., Strahle, U., Kimelman, D., Rosa, F. M.**
1107 **and Peyrieras, N.** (2004). Nodal and Fgf pathways interact through a positive regulatory loop
1108 and synergize to maintain mesodermal cell populations. *Development* **131**, 629-641.

1109 **McNamara, H. M., Guyer, A. M., Jia, B. Z., Parot, V. J., Dobbs, C. D., Schier, A. F., Cohen,**
1110 **A. E. and Lord, N. D.** (2025). Optogenetic control of Nodal signaling patterns. *Development*.

1111 **Mitra, D., Yang, X. and Moffat, K.** (2012). Crystal structures of Aureochrome1 LOV suggest
1112 new design strategies for optogenetics. *Structure* **20**, 698-706.

1113 **Molina, G. A., Watkins, S. C. and Tsang, M.** (2007). Generation of FGF reporter transgenic
1114 zebrafish and their utility in chemical screens. *BMC Dev Biol* **7**, 62.

1115 **Mruk, K., Ciepla, P., Piza, P. A., Alnaqib, M. A. and Chen, J. K.** (2020). Targeted cell
1116 ablation in zebrafish using optogenetic transcriptional control. *Development* **147**.

1117 **Mullins, M. C., Acedo, J. N., Priya, R., Solnica-Krezel, L. and Wilson, S. W.** (2021). The
1118 zebrafish issue: 25 years on. *Development* **148**.

1119 **Nguyen, V. H., Schmid, B., Trout, J., Connors, S. A., Ekker, M. and Mullins, M. C.** (1998).
1120 Ventral and lateral regions of the zebrafish gastrula, including the neural crest progenitors, are
1121 established by a bmp2b/swirl pathway of genes. *Dev Biol* **199**, 93-110.

1122 **Ornitz, D. M. and Itoh, N.** (2015). The Fibroblast Growth Factor signaling pathway. *Wiley*
1123 *Interdiscip Rev Dev Biol* **4**, 215-266.

1124 **Owlarn, S., Klenner, F., Schmidt, D., Rabert, F., Tomasso, A., Reuter, H., Mulaw, M. A.,**
1125 **Moritz, S., Gentile, L., Weidinger, G., et al.** (2017). Generic wound signals initiate
1126 regeneration in missing-tissue contexts. *Nat Commun* **8**, 2282.

**Pal, A. A., Benman, W., Mumford, T. R., Huang, Z., Chow, B. Y. and Bugaj, L. J.** (2023). Optogenetic clustering and membrane translocation of the BcLOV4 photoreceptor. *Proc Natl Acad Sci U S A* **120**, e2221615120.

**Patel, A. L., Yeung, E., McGuire, S. E., Wu, A. Y., Toettcher, J. E., Burdine, R. D. and Shvartsman, S. Y.** (2019). Optimizing photoswitchable MEK. *Proc Natl Acad Sci U S A* **116**, 25756-25763.

**Poss, K. D., Shen, J., Nechiporuk, A., McMahon, G., Thisse, B., Thisse, C. and Keating, M. T.** (2000). Roles for Fgf signaling during zebrafish fin regeneration. *Dev Biol* **222**, 347-358.

**Purvis, J. E. and Lahav, G.** (2013). Encoding and decoding cellular information through signaling dynamics. *Cell* **152**, 945-956.

**Ramachandran, A., Vizan, P., Das, D., Chakravarty, P., Vogt, J., Rogers, K. W., Müller, P., Hinck, A. P., Sapkota, G. P. and Hill, C. S.** (2018). TGF-β uses a novel mode of receptor activation to phosphorylate SMAD1/5 and induce epithelial-to-mesenchymal transition. *Elife* **7**, e31756.

**Ramkumar, N., Richardson, C., O'Brien, M., Butt, F. A., Park, J., Chao, A. T., Bagnat, M., Poss, K. D. and Di Talia, S.** (2025). Phased ERK responsiveness and developmental robustness regulate teleost skin morphogenesis. *Proc Natl Acad Sci U S A* **122**, e2410430122.

**Rauschendorfer, T., Gurri, S., Heggli, I., Maddaluno, L., Meyer, M., Ingles-Prieto, A., Janovjak, H. and Werner, S.** (2021). Acute and chronic effects of a light-activated FGF receptor in keratinocytes in vitro and in mice. *Life Sci Alliance* **4**.

**Reade, A., Motta-Mena, L. B., Gardner, K. H., Stainier, D. Y., Weiner, O. D. and Woo, S.** (2017). TAEL: a zebrafish-optimized optogenetic gene expression system with fine spatial and temporal control. *Development* **144**, 345-355.

**Rebagliati, M. R., Toyama, R., Fricke, C., Haffter, P. and Dawid, I. B.** (1998). Zebrafish nodal-related genes are implicated in axial patterning and establishing left-right asymmetry. *Dev Biol* **199**, 261-272.

**Rogers, K. W., ElGamacy, M., Jordan, B. M. and Müller, P.** (2020). Optogenetic investigation of BMP target gene expression diversity. *Elife* **9**, e58641.

**Rogers, K. W., Lord, N. D., Gagnon, J. A., Pauli, A., Zimmerman, S., Aksel, D. C., Reyon, D., Tsai, S. Q., Joung, J. K. and Schier, A. F.** (2017). Nodal patterning without Lefty inhibitory feedback is functional but fragile. *Elife* **6**, e28785.

**Rogers, K. W. and Müller, P.** (2020). Optogenetic approaches to investigate spatiotemporal signaling during development. In *Gradients and Tissue Patterning*, pp. 37-77.

**Ryan, M. D., King, A. M. and Thomas, G. P.** (1991). Cleavage of foot-and-mouth disease virus polyprotein is mediated by residues located within a 19 amino acid sequence. *J Gen Virol* **72 ( Pt 11)**, 2727-2732.

**Sagner, A. and Briscoe, J.** (2017). Morphogen interpretation: concentration, time, competence, and signaling dynamics. *Wiley Interdiscip Rev Dev Biol* **6**, e271.

**Sako, K., Pradhan, S. J., Barone, V., Inglés-Prieto, Á., Müller, P., Ruprecht, V., Čapek, D., Galande, S., Janovjak, H. and Heisenberg, C. P.** (2016). Optogenetic control of Nodal signaling reveals a temporal pattern of Nodal signaling regulating cell fate specification during gastrulation. *Cell Rep* **16**, 866-877.

**Saul, A. J.*, Rogers, C. E.*, Garmendia-Cedillos, M., Pohida, T. and Rogers, K. W.** (2023). Optogenetic Signaling Activation in Zebrafish Embryos. *Journal of Visualized Experiments*.

**Schmid, B., Furthauer, M., Connors, S. A., Trout, J., Thisse, B., Thisse, C. and Mullins, M. C.** (2000). Equivalent genetic roles for bmp7/snailhouse and bmp2b/swirl in dorsoventral pattern formation. *Development* **127**, 957-967.

**Schwarzkopf, M., Liu, M. C., Schulte, S. J., Ives, R., Husain, N., Choi, H. M. T. and Pierce, N. A.** (2021). Hybridization chain reaction enables a unified approach to multiplexed, quantitative, high-resolution immunohistochemistry and in situ hybridization. *Development* **148**.

**Soh, G. H., Pomreinke, A. P. and Muller, P.** (2020). Integration of Nodal and BMP Signaling by Mutual Signaling Effector Antagonism. *Cell Rep* **31**, 107487.

**Takahashi, F., Yamagata, D., Ishikawa, M., Fukamatsu, Y., Ogura, Y., Kasahara, M., Kiyosue, T., Kikuyama, M., Wada, M. and Kataoka, H.** (2007). AUREOCHROME, a photoreceptor required for photomorphogenesis in stramenopiles. *Proc Natl Acad Sci U S A* **104**, 19625-19630.

**Tamai, T. K., Vardhanabhuti, V., Foulkes, N. S. and Whitmore, D.** (2004). Early embryonic light detection improves survival. *Current Biology* **14**, R104-R105.

**Toettcher, J. E., Weiner, O. D. and Lim, W. A.** (2013). Using optogenetics to interrogate the dynamic control of signal transmission by the Ras/Erk module. *Cell* **155**, 1422-1434.

**Toyooka, T., Hisatomi, O., Takahashi, F., Kataoka, H. and Terazima, M.** (2011). Photoreactions of aureochrome-1. *Biophys J* **100**, 2801-2809.

**Tucker, J. A., Mintzer, K. A. and Mullins, M. C.** (2008). The BMP signaling gradient patterns dorsoventral tissues in a temporally progressive manner along the anteroposterior axis. *Dev Cell* **14**, 108-119.

**Ueda, Y., Miura, Y., Tomishige, N., Sugimoto, N., Murase, M., Kawamura, G., Sasaki, N., Ishiwata, T. and Ozawa, T.** (2022). Mechanistic insights into cancer drug resistance through optogenetic PI3K signaling hyperactivation. *Cell Chem Biol* **29**, 1576-1587 e1575.

**van Boxtel, A. L., Economou, A. D., Heliot, C. and Hill, C. S.** (2018). Long-range signaling activation and local inhibition separate the mesoderm and endoderm lineages. *Dev Cell* **44**, 179-191 e175.

**Vopalensky, P., Pralow, S. and Vastenhouw, N. L.** (2018). Reduced expression of the Nodal co-receptor Oep causes loss of mesendodermal competence in zebrafish. *Development* **145**, dev.158832.

**Whitehead, G. G., Makino, S., Lien, C. L. and Keating, M. T.** (2005). fgf20 is essential for initiating zebrafish fin regeneration. *Science* **310**, 1957-1960.

**Whitmore, D., Foulkes, N. S. and Sassone-Corsi, P.** (2000). Light acts directly on organs and cells in culture to set the vertebrate circadian clock. *Nature* **404**, 87-91.

**Wilcockson, S. G., Guglielmi, L., Araguas Rodriguez, P., Amoyel, M. and Hill, C. S.** (2023). An improved Erk biosensor detects oscillatory Erk dynamics driven by mitotic erasure during early development. *Developmental Cell*.

**Yadav, V., Tolwinski, N. and Saunders, T. E.** (2021). Spatiotemporal sensitivity of mesoderm specification to FGFR signalling in the Drosophila embryo. *Sci Rep* **11**, 14091.

**Zaucker, A., Mitchell, C. A., Coker, H. L. E. and Sampath, K.** (2021). Tools to Image Germplasm Dynamics During Early Zebrafish Development. *Front Cell Dev Biol* **9**, 712503.

**Zhou, X. X., Fan, L. Z., Li, P., Shen, K. and Lin, M. Z.** (2017). Optical control of cell signaling by single-chain photoswitchable kinases. *Science* **355**, 836-842.

**Ziv, L. and Gothilf, Y.** (2006). Circadian time-keeping during early stages of development. *Proc Natl Acad Sci U S A* **103**, 4146-4151.

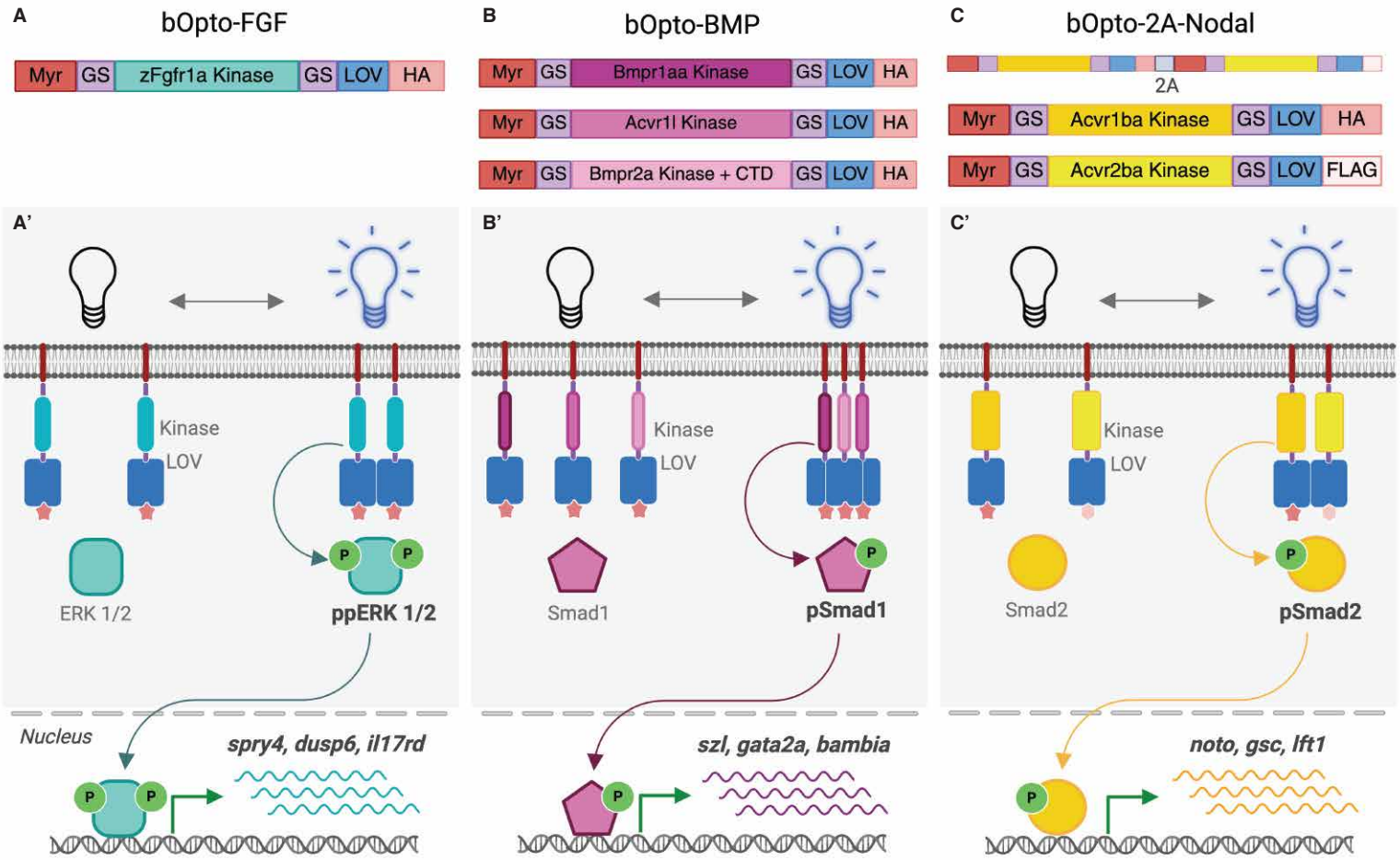


**Figure 1: Optogenetic signaling activator toolkit. A,B,C)** Schematic of constructs used here to activate FGF (A), BMP (B), and Nodal (C) signaling. Myr = myristoylation motif, GS = glycine/serine linker, LOV = light oxygen voltage-sensing domain, HA = hemagglutinin tag, FLAG = FLAG epitope. The single-transcript bOpto-2A-Nodal construct (C) follows the same design as -FGF and -BMP, except the type I (Acvr1ba) and type II (Acvr2ba) components are connected via a 2A peptide sequence (gray). **A',B',C')** Optogenetic strategy to activate FGF (A'), BMP (B'), and Nodal (C') signaling. Blue light-dimerizing LOV domains are fused to myristoylated receptor kinase domains. Blue light exposure should lead to receptor kinase interactions, signaling effector phosphorylation, and activation of target genes.

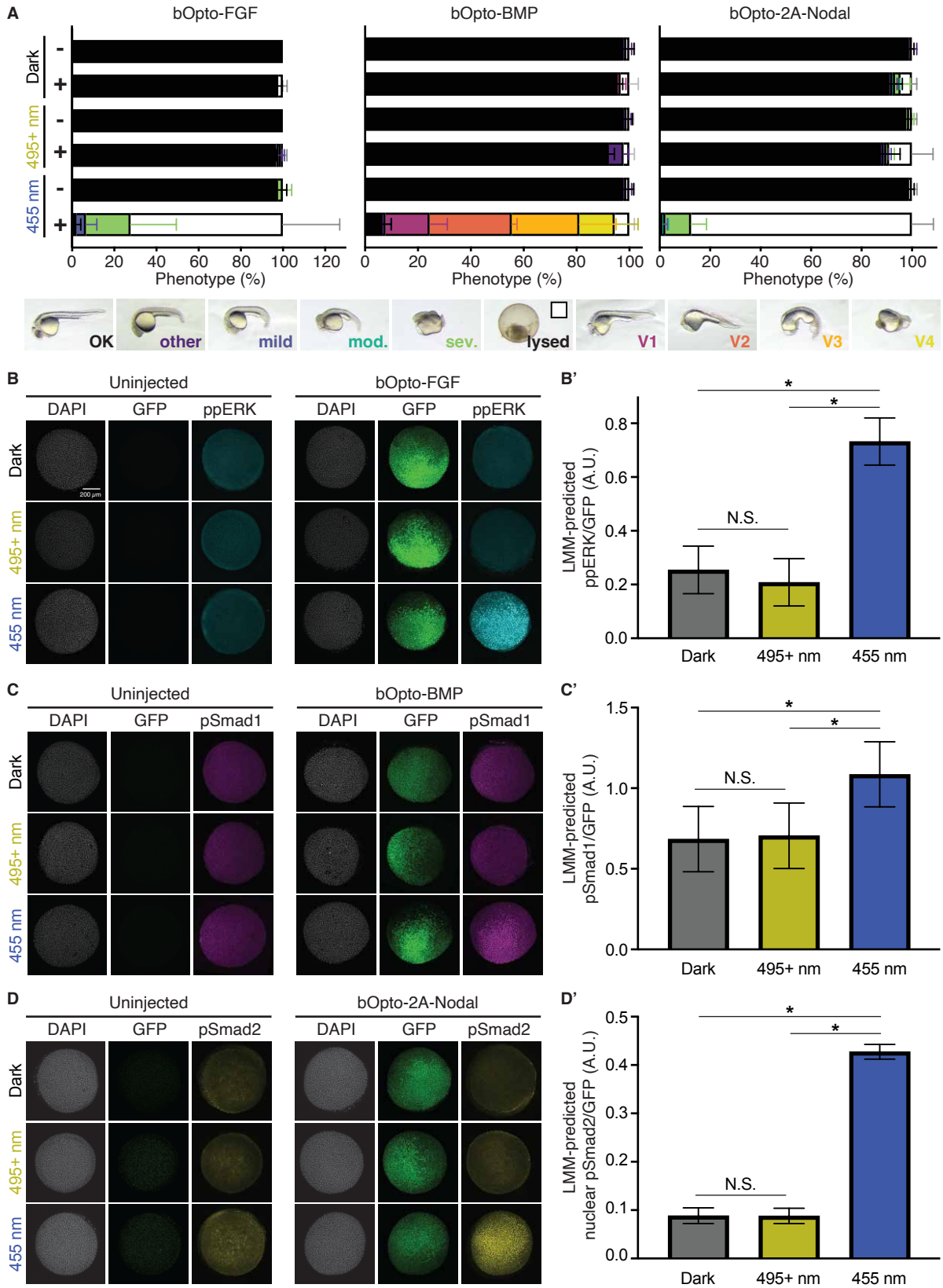


**Figure 2: Wavelength-dependent activation of FGF, BMP, & Nodal signaling. A)** Uninjected (-) embryos and embryos injected (+) at the one-cell stage with the indicated mRNA were exposed to dark, 495+ nm light (18.51 W/m$^2$), or 455 nm light (50 W/m$^2$) starting ~2 hours post-fertilization (hpf). Phenotypes were scored at 1 day post-fertilization (dpf) (N = 3; Supp. Fig. 2; Mean +/- SD). **B,C,D)** Uninjected embryos and embryos injected with the indicated *bOpto* + *GFP* mRNA were exposed to dark, 495+ nm light, or 455 nm light starting at early gastrulation (50% epiboly - shield) for 30 min. HCR-IF was used to detect phosphorylated signaling effectors (ppERK, pSmad1, and pSmad2 reflect FGF, BMP, and Nodal signaling, respectively). Scale bar is 200 $\mu$m. **B',C',D')** Quantification of experiments shown in B,C,D. Linear-mixed model-predicted least squared means of GFP-normalized phosphorylated effector signal +/- SEM. D' shows nuclear signal only. (N = 3, * indicates $p < 0.05$; Supp. Figs. 3 & 4).

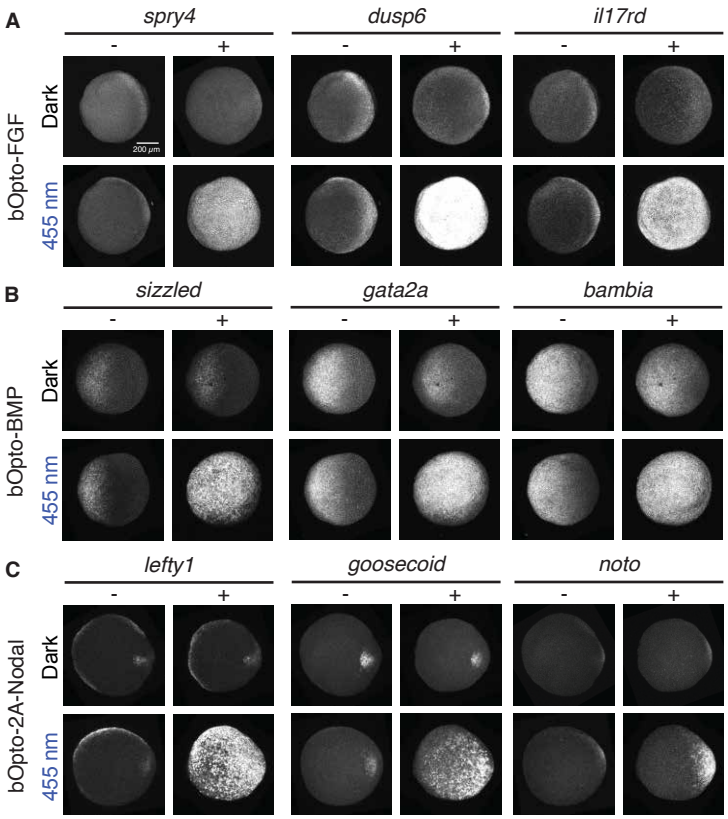


**Figure 3: bOpto tools activate target gene expression.** Uninjected embryos (-) and embryos injected (+) at the one-cell stage with mRNA encoding bOpto-FGF **(A)**, bOpto-BMP **(B)**, or bOpto-2A-Nodal **(C)** were exposed to 455 nm light (50 W/m$^2$, bottom rows) or dark (top rows) for 2 hours starting before gastrulation (dome - 30% epiboly). Multiplexed HCR-FISH was used to detect expression of the indicated pathway target genes. (N = 3; Scale bar is 200 $\mu$m).

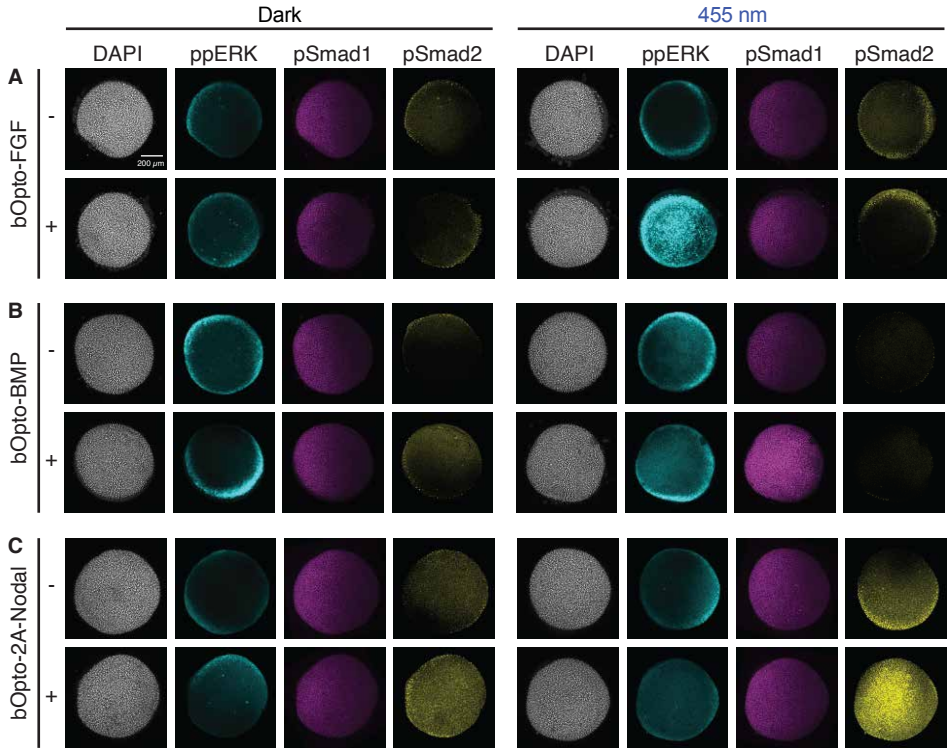


**Figure 4: Pathway-specific optogenetic activation of FGF, BMP, & Nodal signaling.** Uninjected embryos (-) and embryos injected (+) at the one-cell stage with mRNA encoding bOpto-FGF **(A)**, bOpto-BMP **(B)**, or bOpto-2A-Nodal **(C)** were exposed to dark (left panel) or 455 nm light (50 W/m$^2$, right panel) for 30 minutes starting at gastrulation (50% epiboly - shield). Triple IF was used to simultaneously detect phosphorylated signaling effectors (ppERK, pSmad1, and pSmad2 reflect FGF, BMP, and Nodal signaling, respectively). (N = 3; Supp. Fig. 5; Scale bar is 200 $\mu$m).

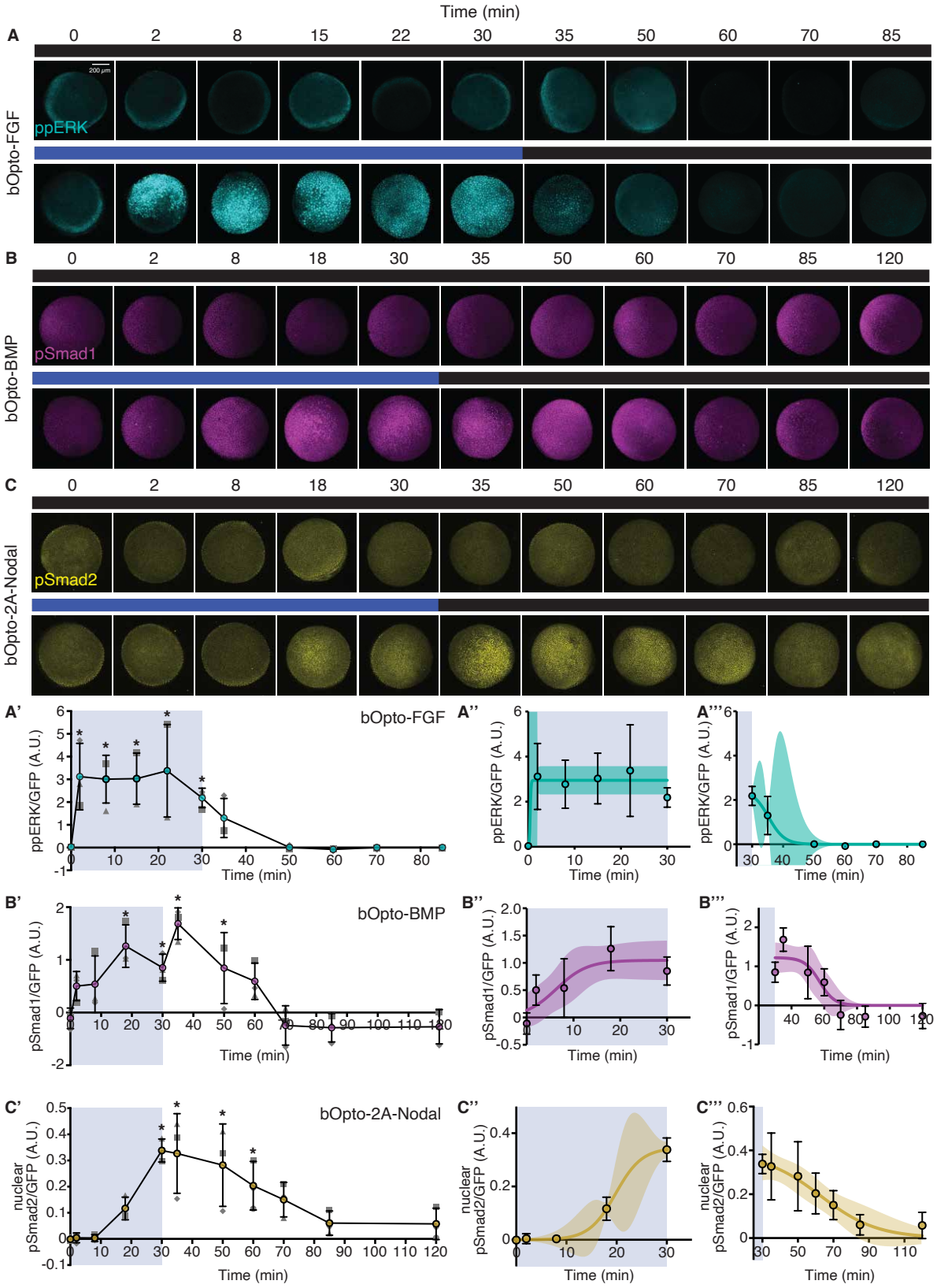


**Figure 5: On/off kinetics of optogenetic signaling activator toolkit.** Embryos were injected at the one-cell stage with mRNA encoding *GFP* and either *bOpto-FGF*, *bOpto-BMP*, or *bOpto-2A-Nodal* . **A,B,C)** Starting at early gastrulation (50% epiboly - shield), embryos were either kept in the dark (top row) or exposed to 455 nm light (50 W/m$^2$) light for 30 min (bottom row) and fixed during and after exposure. HCR-IF was used to detect activated signaling effectors (ppERK, pSmad1, and pSmad2 reflect FGF, BMP, and Nodal signaling, respectively). (N = 3; Scale bar is 200 $\mu$m). **A',B',C')** Quantification of experiments shown in A-C. Signal was GFP-normalized and subtracted against dark time-matched controls (N = 3; each N indicated by matched shape; Supp. Fig. 6 & 7; Mean +/- SD; * indicates $p < 0.05$ when compared to time = 0 min). **A''- C'', A'''-C''')** A three-parameter logistic regression was fit to the 0-30 min data (A''-C'') or the >= 30 min data (A'''-C'''). (N = 3; Mean +/- SD; Supplementary Materials; solid line represents predicted curve fit +/- 95% CI).

**A**

| Irradiance (W/m$^2$) | All | 0.02 | 0.05 | 0.15 | 0.46 | 1.39 | 4.17 | 12.50 | 50.00 |
|---|---|---|---|---|---|---|---|---|---|
| Dosage (J/m$^2$) | FGF (5 min) | 4.63 | 13.89 | 46.30 | 138.89 | 416.67 | 1250.00 | 3750.00 | 15000.00 |
| | BMP, Nodal (25 min) | 23.15 | 69.44 | 231.48 | 694.44 | 2083.33 | 6250.00 | 18750.00 | 75000.00 |

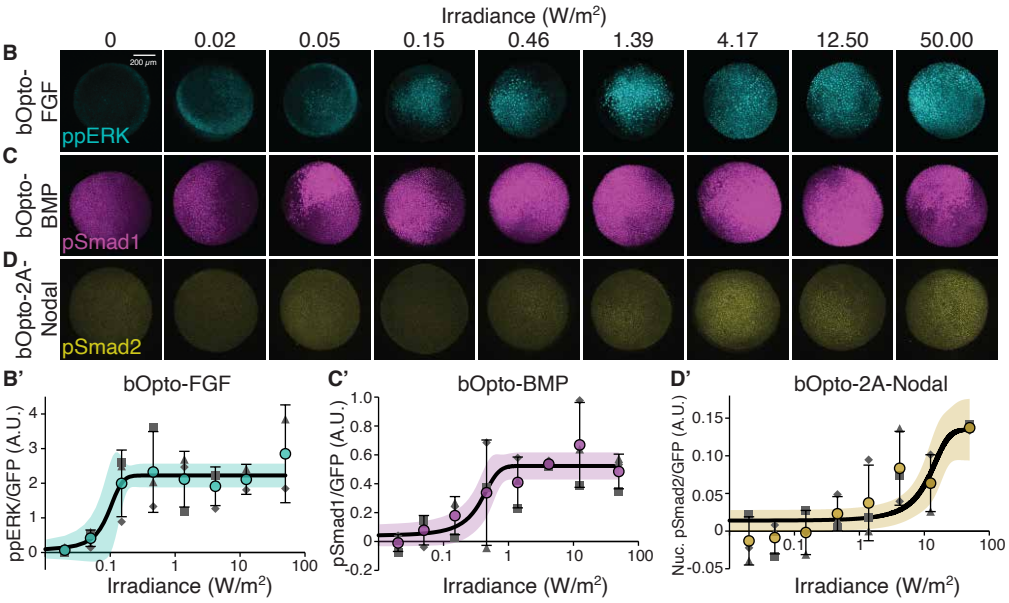


| Parameter | Value | 95% CI |
|---|---|---|
| $R^2$ | 0.748 | |
| $I_{20}$ | 0.05 | 0.00-0.11 |
| $I_{50}$ | 0.09 | 0.03-0.15 |
| $I_{90}$ | 0.15 | 0.05-0.25 |

| Parameter | Value | 95% CI |
|---|---|---|
| $R^2$ | 0.678 | |
| $I_{20}$ | 0.16 | -0.03-0.35 |
| $I_{50}$ | 0.35 | 0.17-0.53 |
| $I_{90}$ | 0.67 | 0.26-1.08 |

| Parameter | Value | 95% CI |
|---|---|---|
| $R^2$ | 0.578 | |
| $I_{20}$ | 3.90 | -0.27-8.06 |
| $I_{50}$ | 11.00 | 5.54-16.45 |
| $I_{90}$ | 22.25 | 6.12-38.38 |

**Figure 6: Irradiance sensitivity of optogenetic toolkit. A)** Table of irradiance and corresponding light dosage values used in B-D'. **B,C,D)** Embryos were injected at the one-cell stage with mRNA encoding *GFP* and either *bOpto-FGF* (B), *bOpto-BMP* (C), or *bOpto-2A-Nodal* (D). Starting at early gastrulation (50% epiboly - shield), embryos were exposed to 455 nm light at the indicated irradiance for 5 min (bOpto-FGF, B) or 25 min (bOpto-BMP and -2A-Nodal, C and D). HCR-IF was used to detect phosphorylated signaling effectors (ppERK, pSmad1, and pSmad2 reflect FGF, BMP, and Nodal signaling, respectively; Scale bar is 200 $\mu$m). **B',C',D')** Quantification of experiments in B-D. Signal was GFP-normalized and subtracted against dark controls. A three-parameter logistic regression was fit to the data. (N = 2-3; each N indicated by matched shape; Mean +/- SD; Supp. Fig. 8 & 9; solid line represents predicted curve fit +/- 95% CI; D' shows nuclear signal only). Tables indicate goodness of fit ($R^2$), the predicted irradiance (with 95% CI) at which 20 ($I_{20}$), 50 ($I_{50}$), and 90% ($I_{90}$) of the curve's upper asymptote is reached (Supplementary Materials).

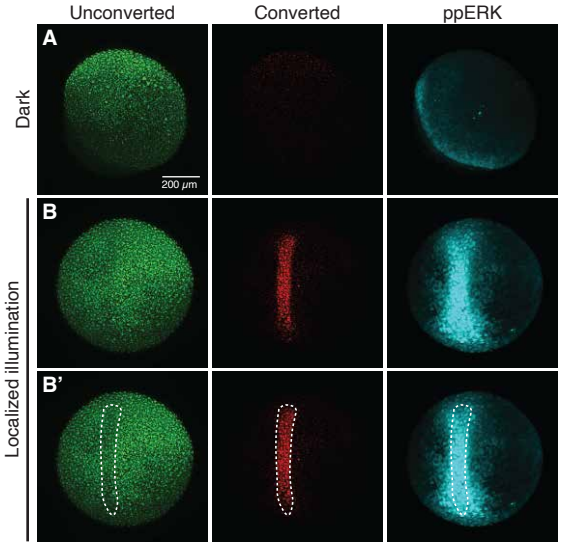


**Figure 7: Spatially localized FGF signaling activation.** Embryos were injected at the one-cell stage with mRNA encoding the green-to-red photoconvertible fluorescent protein *nls-Kaede* and *bOpto-FGF*. At early gastrulation (shield) embryos were either kept in the dark **(A)** or illuminated locally with 405 and 445 nm confocal lasers **(B,B')**. HCR-IF was used to detect ppERK. Dotted white line in B' outlines photoconverted Kaede in embryo shown in B. (Supp. Fig. 10; Scale bar is 200 $\mu$m).

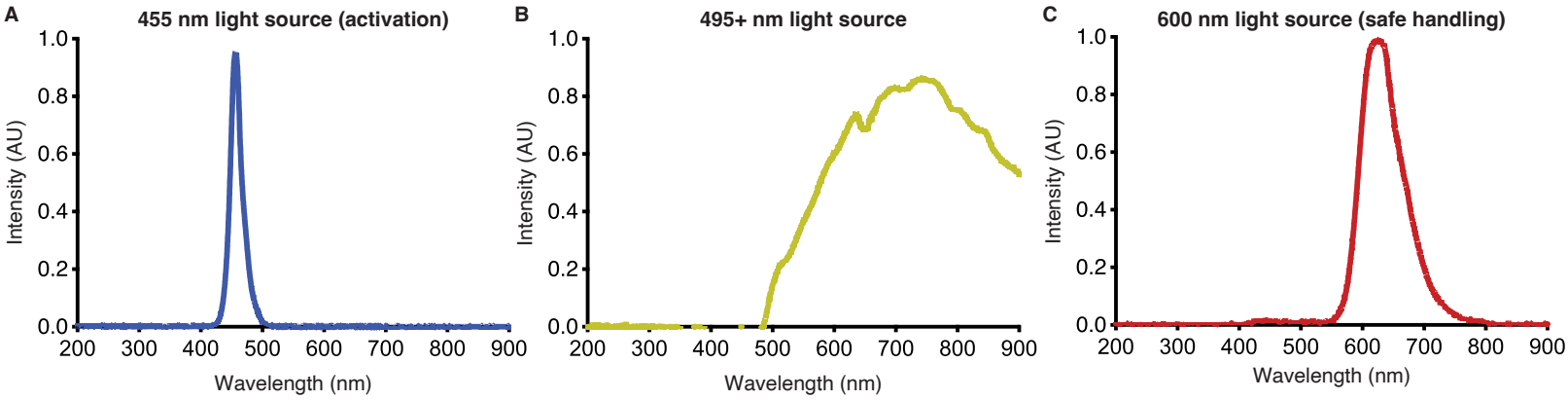


**Supplementary Figure 1: Light source spectra.** Measured spectra for **A)** the 455 nm light used in uniform blue light exposure experiments (all figures except Fig. 7), **B)** the 495+ nm used in Figs. 2 and Supp. Figs. 2, 3, 4, & 12, and **C)** the 600 nm light source used to avoid inadvertent signaling activation during handling of embryos expressing bOpto constructs.

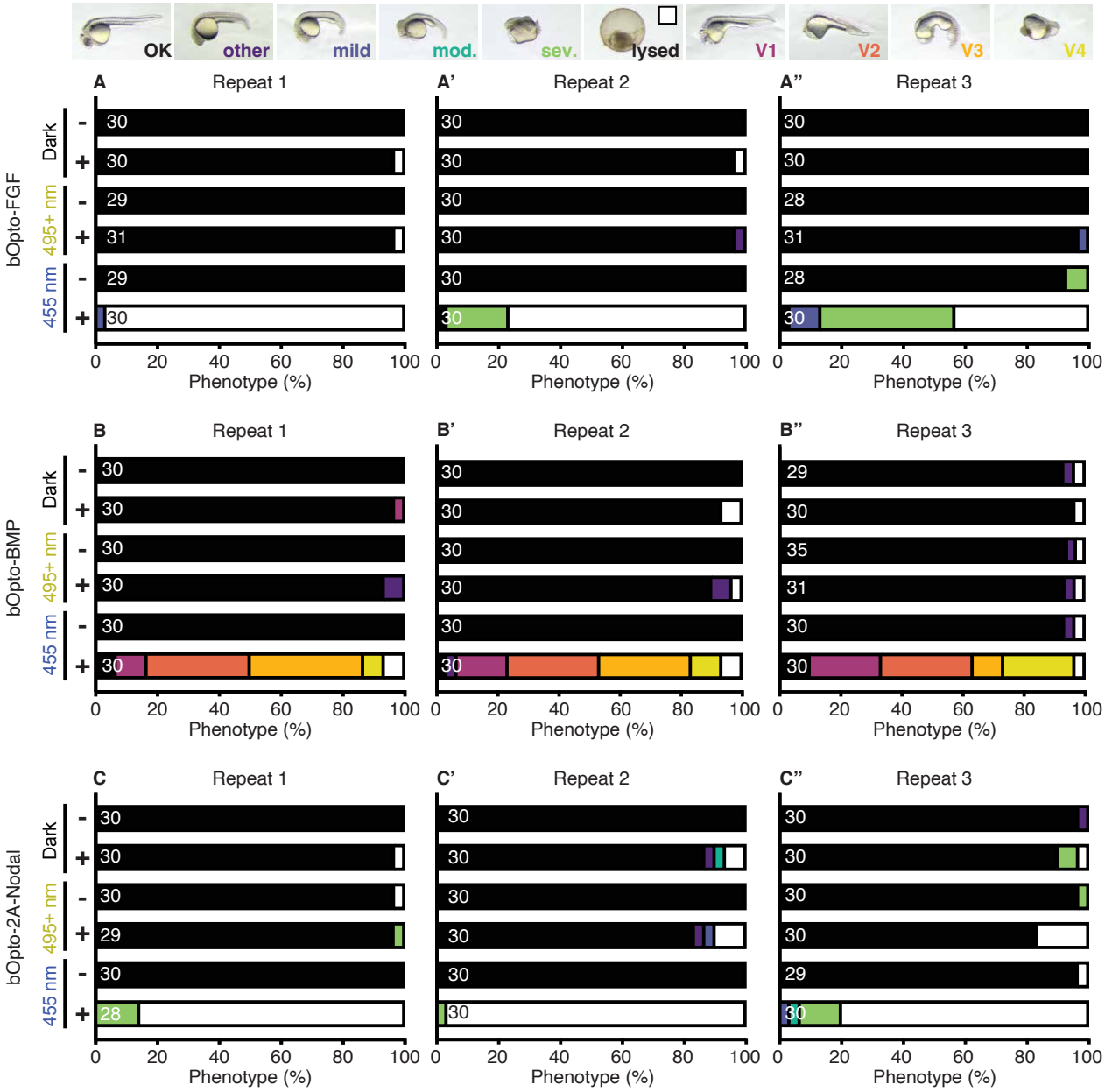


**Supplementary Figure 2: Wavelength-dependent activation of FGF, BMP, & Nodal signaling experiment repeats. A-C")** Uninjected embryos (-) and embryos injected (+) at the one-cell stage with the *bOpto-FGF* (A-A"), *bOpto-BMP* (B-B"), or *bOpto-2A-Nodal* (C-C") mRNA were exposed to dark, 495+ nm light (18.51 W/m$^2$), or 455 nm light (50 W/m$^2$) starting 1.5-2 hours post-fertilization. Phenotypes were scored at 1 day post-fertilization. Individual repeats are shown. Numbers indicate the total number of embryos scored in each condition for that experiment. Figure 2A shows the combined data from these three repeats. Phenotype legend images shown here are the same images shown in Figure 2A.

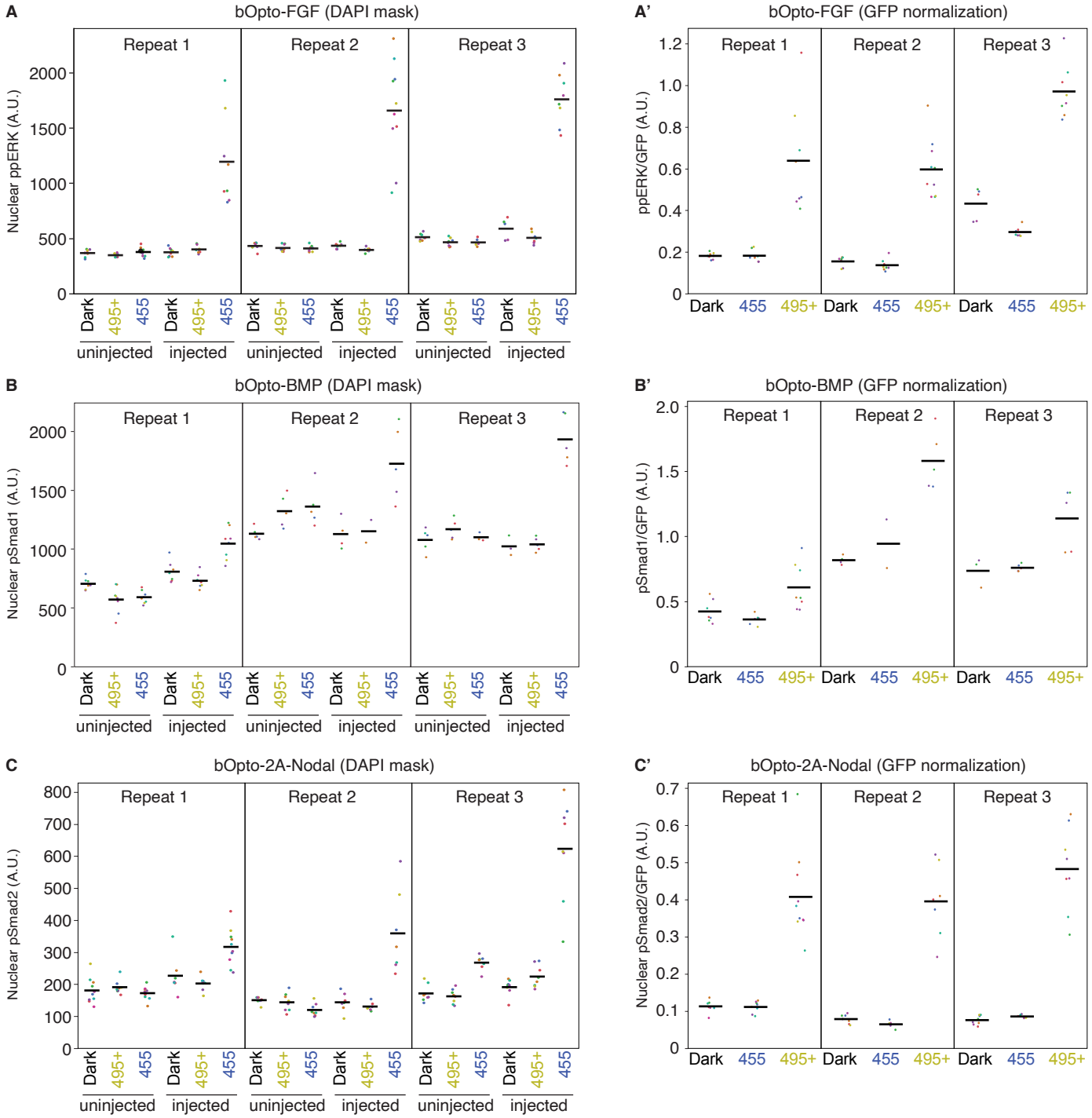


**Supplementary Figure 3: Wavelength-dependent activation of FGF, BMP, & Nodal signaling quantification I. A-C')** Embryos injected at the one-cell stage with the indicated mRNA (+ *GFP* mRNA) were exposed to dark, 495+ nm light (18.51 W/m$^2$), or 455 nm light (50 W/m$^2$) starting at early gastrulation (50% epiboly - shield) for 30 min. HCR-IF was used to detect activated signaling effectors (ppERK, pSmad1, and pSmad2 reflect FGF, BMP, and Nodal signaling, respectively). A,B,C) Raw phosphorylated signaling effector intensity was measured in each DAPI-positive nuclear pixel. Each dot represents the median nuclear pixel intensity in one embryo. Black lines represent the mean nuclear intensity of all embryos in the indicated condition. A', B') GFP-normalized phosphorylated effector signal in each GFP-positive pixel. Each dot represents the median GFP-normalized pixel signal in one embryo. Black lines represent the mean GFP-normalized signal of all embryos in the indicated condition. C') pSmad2 intensity in each DAPI + GFP-positive pixel was divided by the corresponding GFP intensity. Each dot represents the median GFP-normalized nuclear pixel signal in one embryo. Black lines represent the mean GFP-normalized nuclear signal of all embryos in the indicated condition.

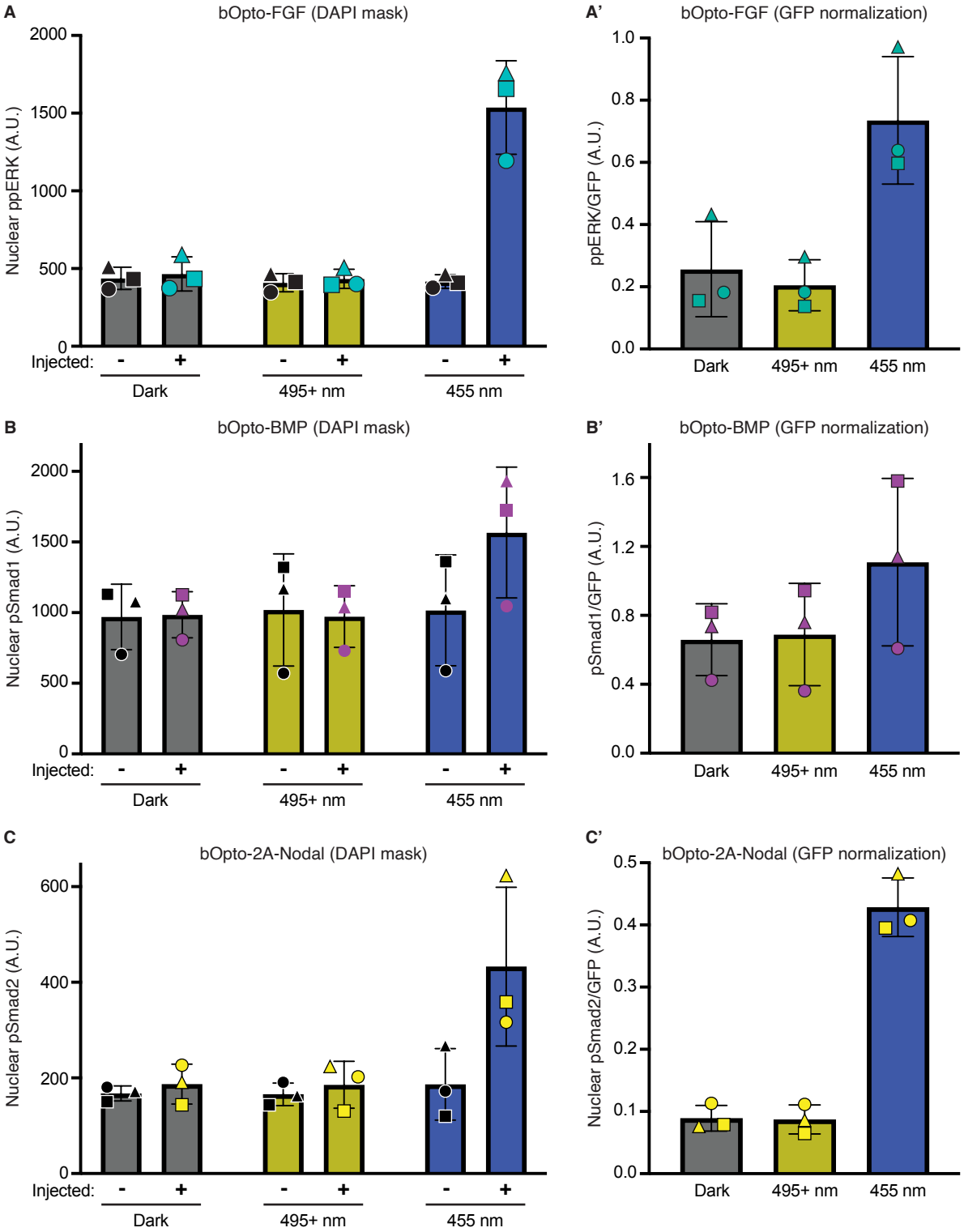


**Supplementary Figure 4: Wavelength-dependent activation of FGF, BMP, & Nodal signaling quantification II.** Uninjected embryos (-) and embryos injected (+) at the one-cell stage with the indicated mRNA + *GFP* mRNA were exposed to dark, 495+ nm light, or 455 nm light starting at early gastrulation (50% epiboly - shield) for 30 min. HCR-IF was used to detect phosphorylated signaling effectors (ppERK, pSmad1, and pSmad2 reflect FGF, BMP, and Nodal signaling, respectively). **A,B,C)** Raw phosphorylated signaling effector intensity was measured in each DAPI-positive nuclear pixel. Each symbol (square, circle, triangle) represents the averaged median intensities from all embryos in one experimental repeat. **A',B')** Phosphorylated signaling effector intensity in each GFP-positive pixel was divided by the corresponding GFP intensity. Each symbol (square, circle, triangle) represents the averaged median GFP-normalized signal from all embryos in one experimental repeat. **C')** pSmad2 intensity in each DAPI + GFP-positive pixel was divided by the corresponding GFP intensity. Each symbol (square, circle, triangle) represents the averaged median GFP-normalized signal from all embryos in one experimental repeat.

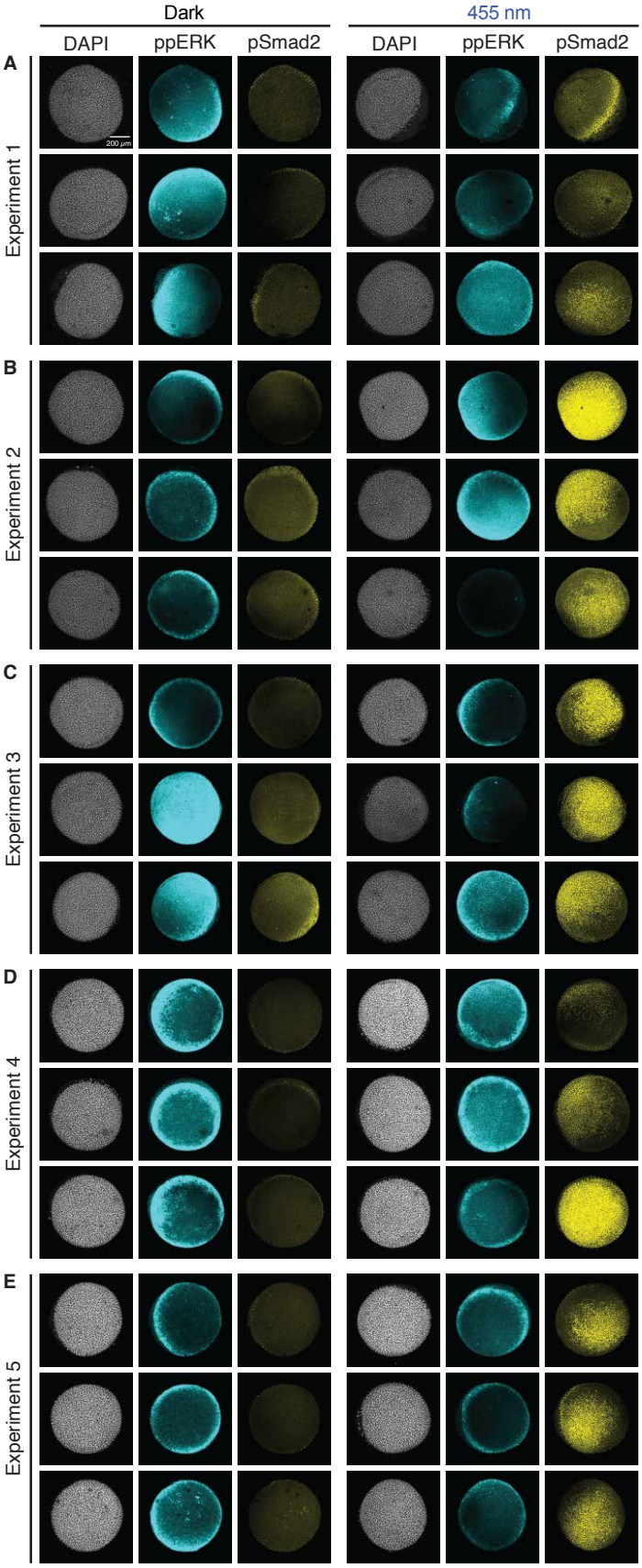


**Supplementary Figure 5: bOpto-2A-Nodal triple immunofluorescence repeats. A-E)** Embryos injected at the one-cell stage with mRNA encoding *bOpto-2A-Nodal* exposed to dark (left panel) or 455 nm light (50 W/m$^2$, right panel) starting at early gastrulation (50% epiboly - shield stage) for 30 min. Triple IF staining was used to simultaneously detect activated signaling effectors (pSmad1, ppERK, and pSmad2 reflecting BMP, FGF, and Nodal signaling, respectively). Only ppERK and pSmad2 shown here. Three bOpto-2A-Nodal-expressing embryos per condition from five experimental repeats are shown. (Scale bar is 200 $\mu$m).

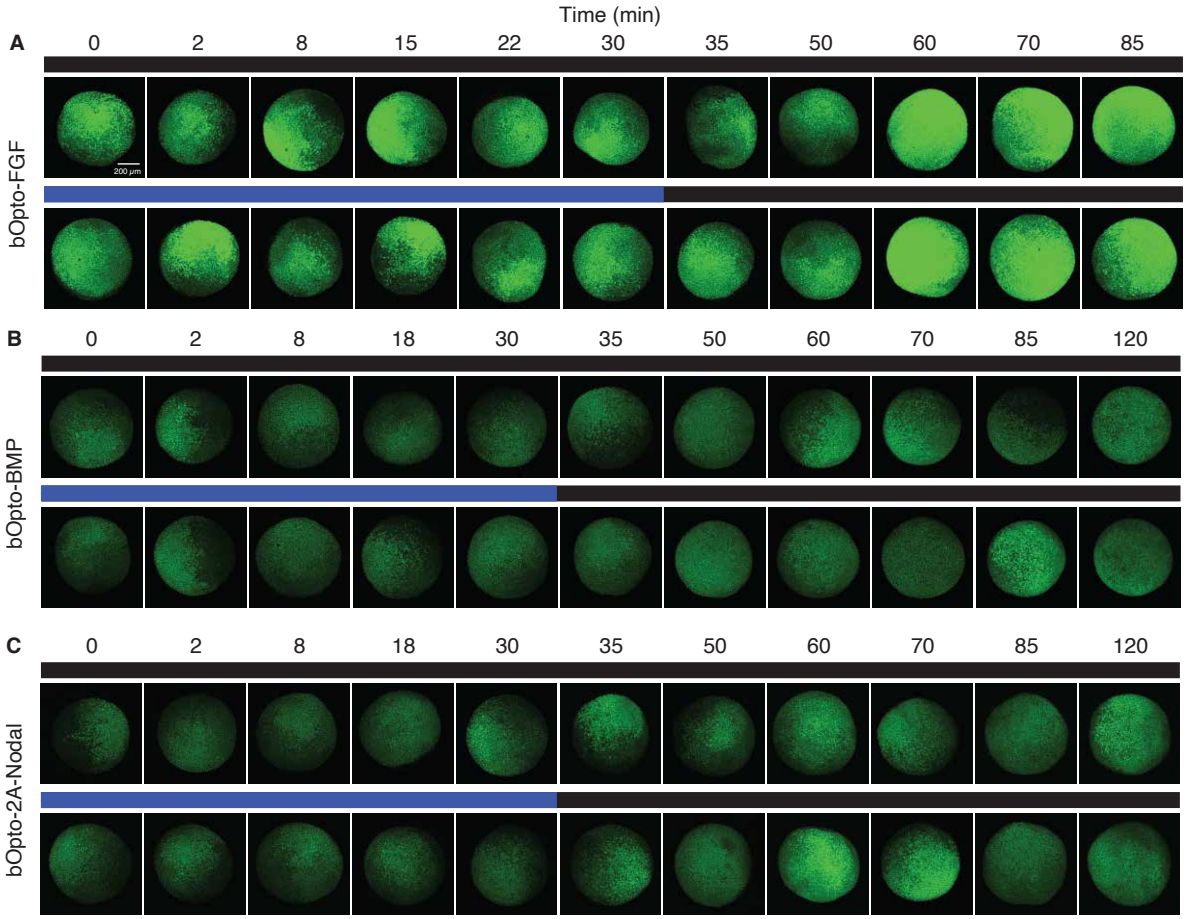


**Supplementary Figure 6: Co-injected GFP signal used for quantification of on / off kinetics. A-C)** Embryos were injected at the one-cell stage with mRNA encoding *GFP* and either *bOpto-FGF* (A), *bOpto-BMP* (B), or *bOpto-2A-Nodal* (C). Starting at early gastrulation (50% epiboly - shield), embryos were exposed to 455 nm light (50 W/m$^2$) for 30 min and fixed at different time points during and after exposure. HCR-IF staining used to detect activated signaling effectors is shown in Fig. 5 (ppERK, pSmad1, and pSmad2 reflect FGF, BMP, and Nodal signaling, respectively). HCR-IF signal was normalized voxel-wise based on co-injected GFP intensity shown here (see Supp. Fig. 7). GFP images correspond to representative IF images shown in Fig. 5. (Scale bar is 200 $\mu$m).

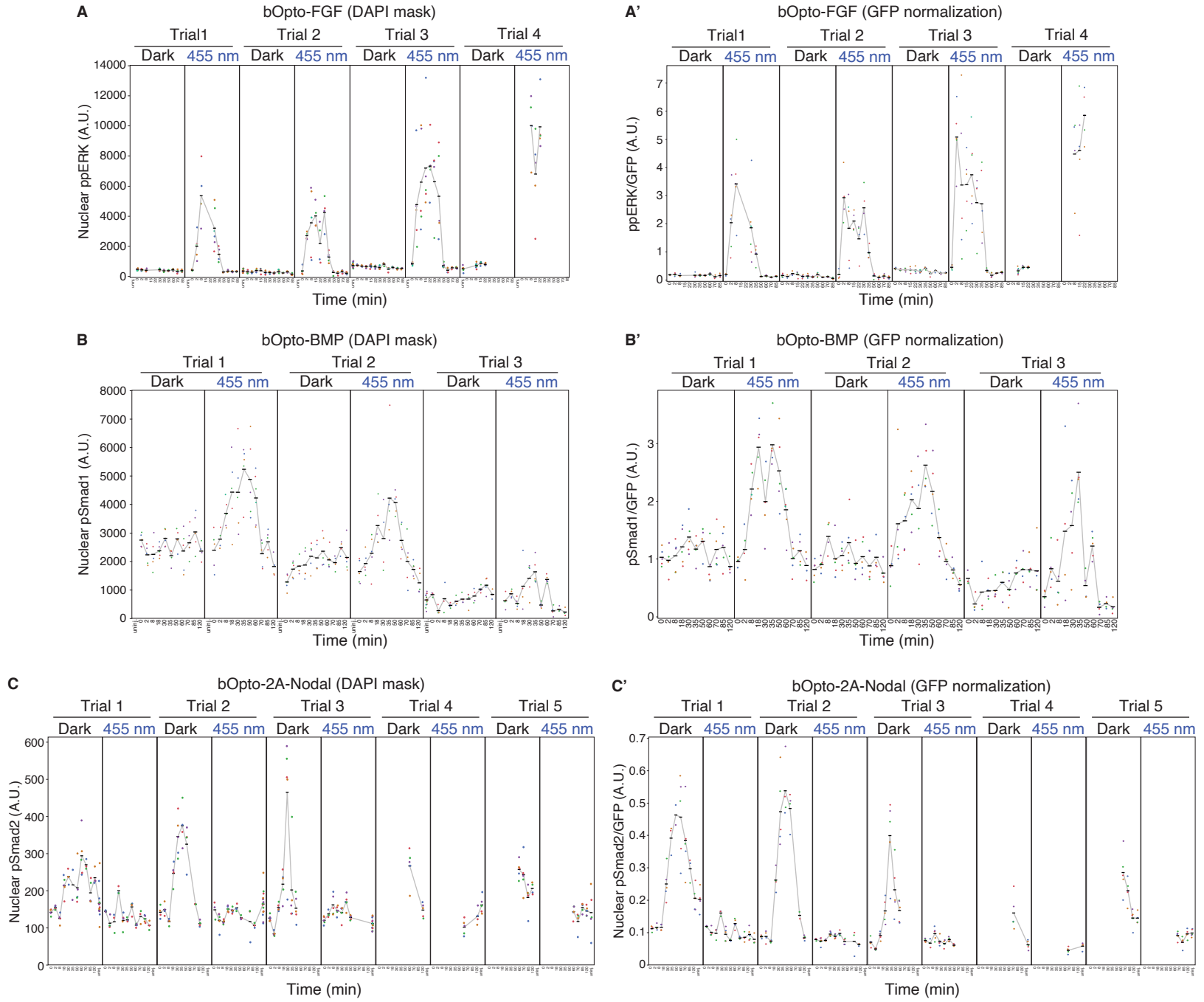


**Supplementary Figure 7: Quantification of optogenetic signaling activator toolkit on/off kinetics.** Embryos were injected at the one-cell stage with mRNA encoding *GFP* and either *bOpto-FGF* (A,A'), *bOpto-BMP* (B,B'), or *bOpto-2A-Nodal* (C,C'). Starting at early gastrulation (50% epiboly - shield), embryos were exposed to 455 nm light (50 W/m$^2$) for 30 min and fixed during and after exposure. Three full repeats were performed across 3-5 trials. HCR-IF staining used to detect phosphorylated signaling effectors is shown in Fig. 5 (ppERK, pSmad1, and pSmad2 reflect FGF, BMP, and Nodal signaling, respectively). **A,B,C)** Raw phosphorylated signaling effector intensity was measured in each DAPI-positive nuclear pixel. Each dot represents the median nuclear pixel intensity in one embryo. Black lines represent the mean nuclear intensity of all embryos in the indicated condition. **A',B')** Phosphorylated siganling effector intensity in each GFP-positive pixel was divided by the corresponding GFP intensity. Each dot represents the median GFP-normalized pixel signal in one embryo. Black lines represent the mean GFP-normalized signal of all embryos in the indicated condition. **C')** pSmad2 intensity in each DAPI + GFP-positive pixel was divided by the corresponding GFP intensity. Each dot represents the median GFP-normalized nuclear pixel signal in one embryo. Black lines represent the mean GFP-normalized nuclear signal of all embryos in the indicated condition.

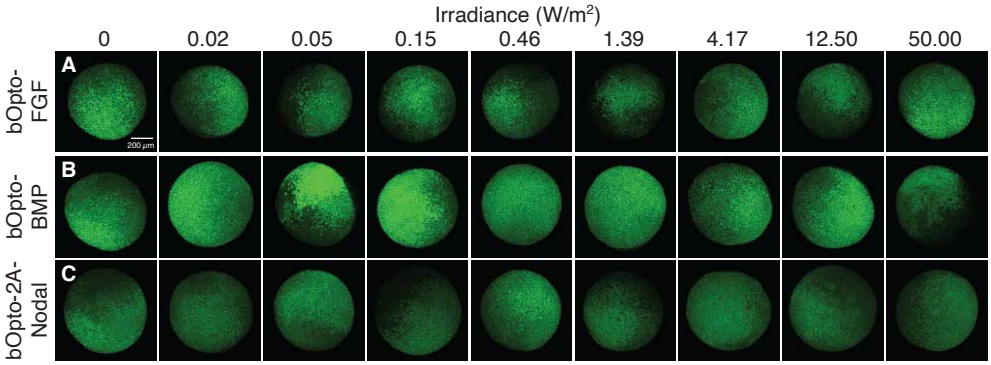


**Supplementary Figure 8: Co-injected GFP signal used for quantification of irradiance dependence HCR-IF. A-C)** Embryos were injected at the one-cell stage with mRNA encoding *GFP* and either *bOpto-FGF* (A), *bOpto-BMP* (B), or *bOpto-2A-Nodal* (C). Starting at early gastrulation (50% epiboly - shield), embryos were exposed to 455 nm light (50 W/m$^2$) at the indicated irradiances for 5 min (bOpto-FGF) or 25 min (bOpto-BMP and -2A-Nodal). HCR-IF staining used to detect phosphorylated signaling effectors is shown in Fig. 6 (ppERK, pSmad1, and pSmad2 to reflect FGF, BMP, and Nodal signaling, respectively). HCR-IF signal was normalized based on co-injected GFP intensity shown here; GFP images correspond to representative images shown in Fig. 6. (Scale bar is 200 $\mu$m).

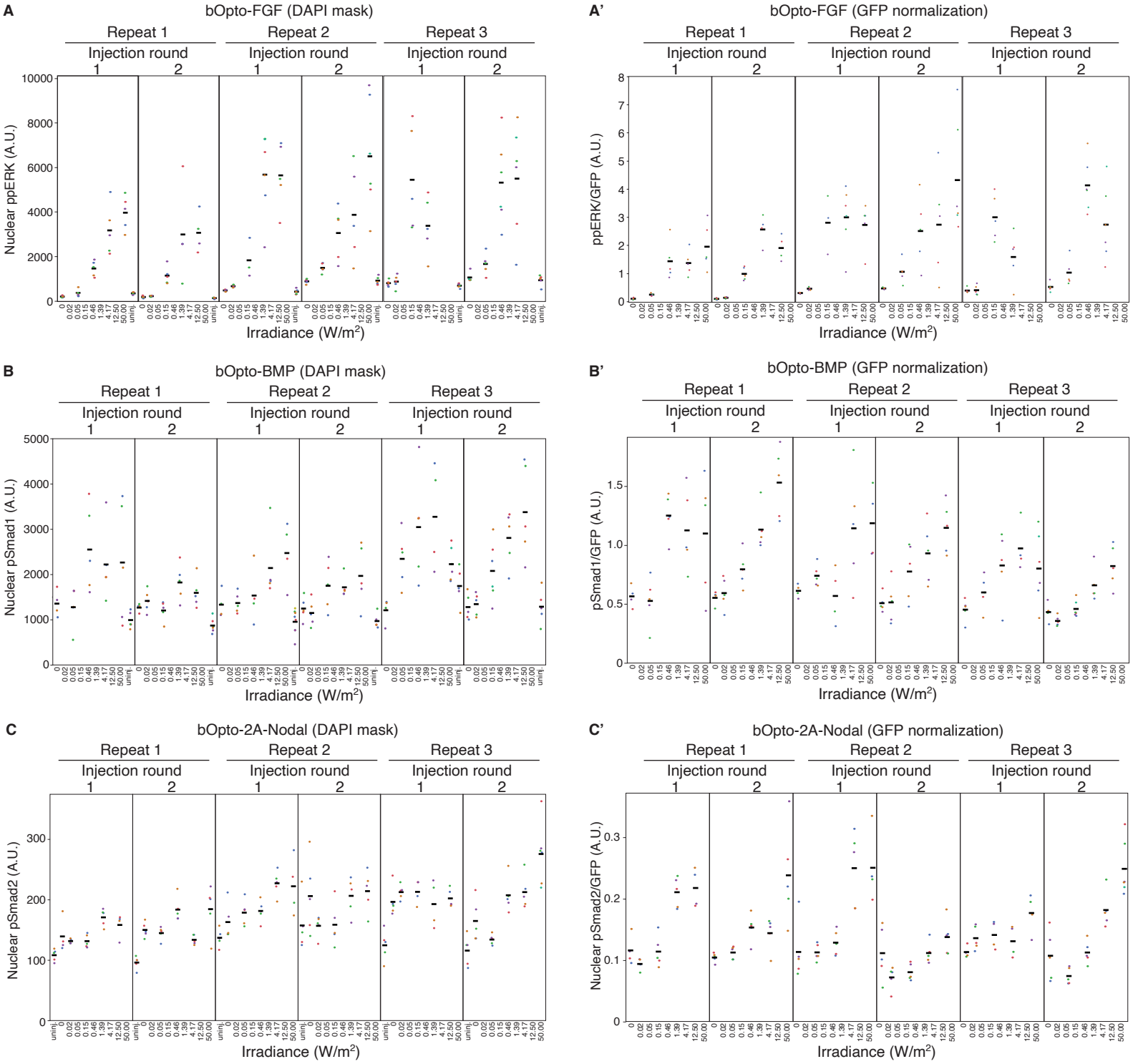


**Supplementary Figure 9: Quantification of light irradiance dependence.** Embryos were injected at the one-cell stage with mRNA encoding *GFP* and either *bOpto-FGF* (A,A'), *bOpto-BMP* (B,B'), or *bOpto-2A-Nodal* (C,C'). At early gastrulation (50% epiboly - shield), embryos were exposed to 455 nm light (50 W/m$^2$) at the indicated irradiance for 5 min (bOpto-FGF) or 25 min (bOpto-BMP and -2A-Nodal). HCR-IF was used to detect phosphorylated signaling effectors (ppERK, pSmad1, and pSmad2 reflect FGF, BMP, and Nodal signaling, respectively). **A,B,C)** Raw phosphorylated signaling effector intensity was measured in each DAPI-positive nuclear pixel. Each dot represents the median nuclear pixel intensity in one embryo. Black lines represent the mean nuclear intensity of all embryos in the indicated condition. **A',B')** Phosphorylated siganling effector intensity in each GFP-positive pixel was divided by the corresponding GFP intensity. Each dot represents the median GFP-normalized pixel signal in one embryo. Black lines represent the mean GFP-normalized signal of all embryos in the indicated condition. **C')** pSmad2 intensity in each DAPI + GFP-positive pixel was divided by the corresponding GFP intensity. Each dot represents the median GFP-normalized nuclear pixel signal in one embryo. Black lines represent the mean GFP-normalized nuclear signal of all embryos in the indicated condition.

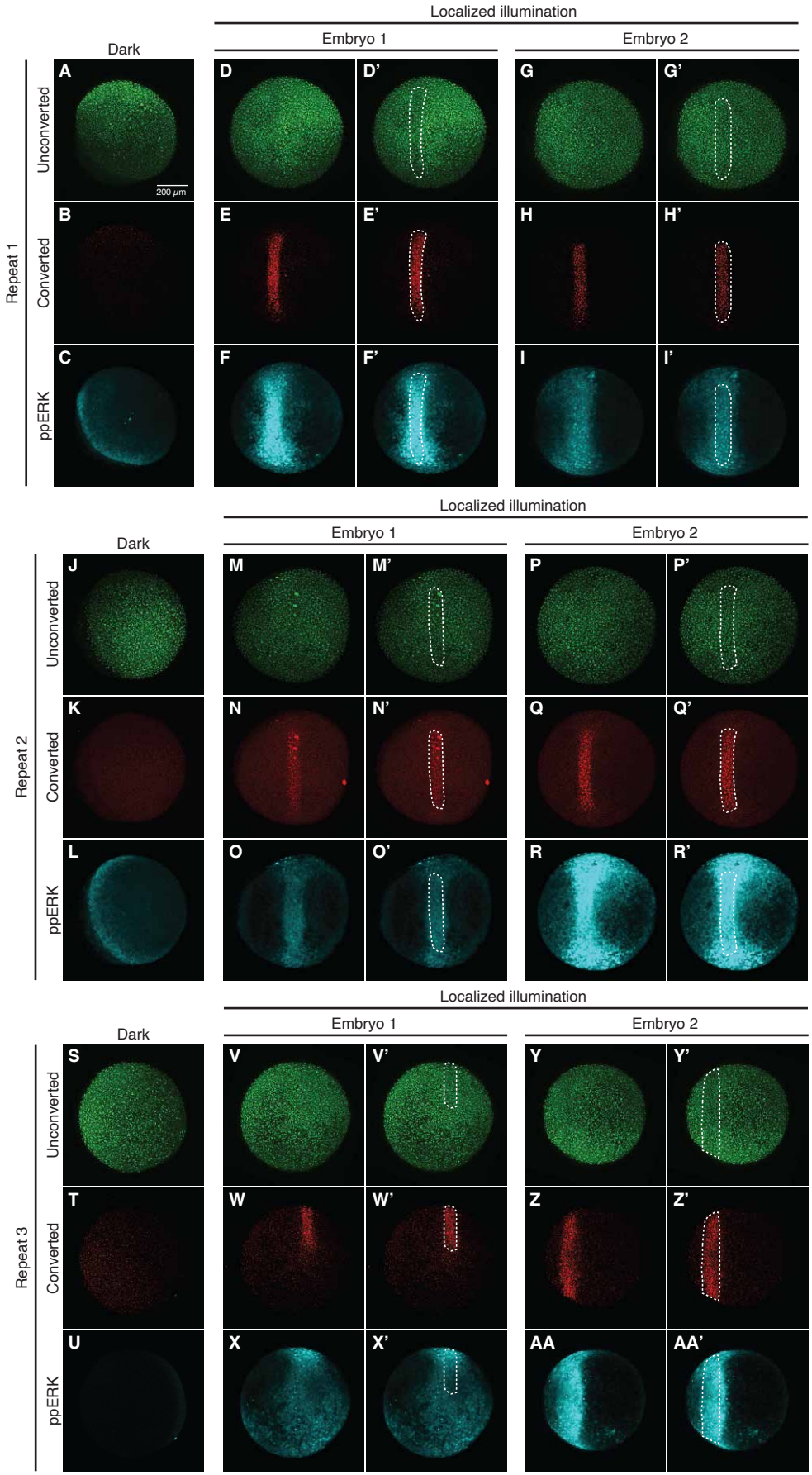


**Supplementary Figure 10: Spatially localized FGF signaling activation repeats.** Embryos were injected at the one-cell stage with mRNA encoding the green-to-red photoconvertible fluorescent proteins *nls-Kaede* and *bOpto-FGF*. At early gastrulation embryos were either kept in the dark (**A-C, J-L, S-U**) or illuminated locally with 405 and 445 nm confocal lasers. HCR-IF was used to detect ppERK. Two representative exposed embryos from three repeats shown (**D-I', M-R', V-AA'**, respectively). Dotted white lines outline photoconverted Kaede from images to the left. A-F' are shown in Fig. 7. (Scale bar is 200 $\mu$m).

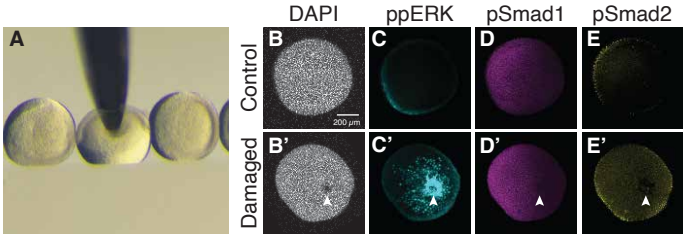


**Supplementary Figure 11: Damage-activated ERK phosphorylation at gastrulation stage. A-E)** Wild type, uninjected zebrafish embryos were dechorionated with pronase at the one-cell stage. At early gastrulation (~50% epiboly), embryos were left undamaged (B,C,D,E) or firmly poked with a metal probe (A,B',C',D',E') and fixed 20 min later. Triple IF + DAPI staining was used to detect nuclei (B, B') and phosphorylated signaling effectors ppERK (C,C'), pSmad1 (D,D') and, pSmad2 (E,E'). Damage visible in the DAPI channel correlates with ERK phosphorylation (arrowheads). (Scale bar is 200 $\mu$m).

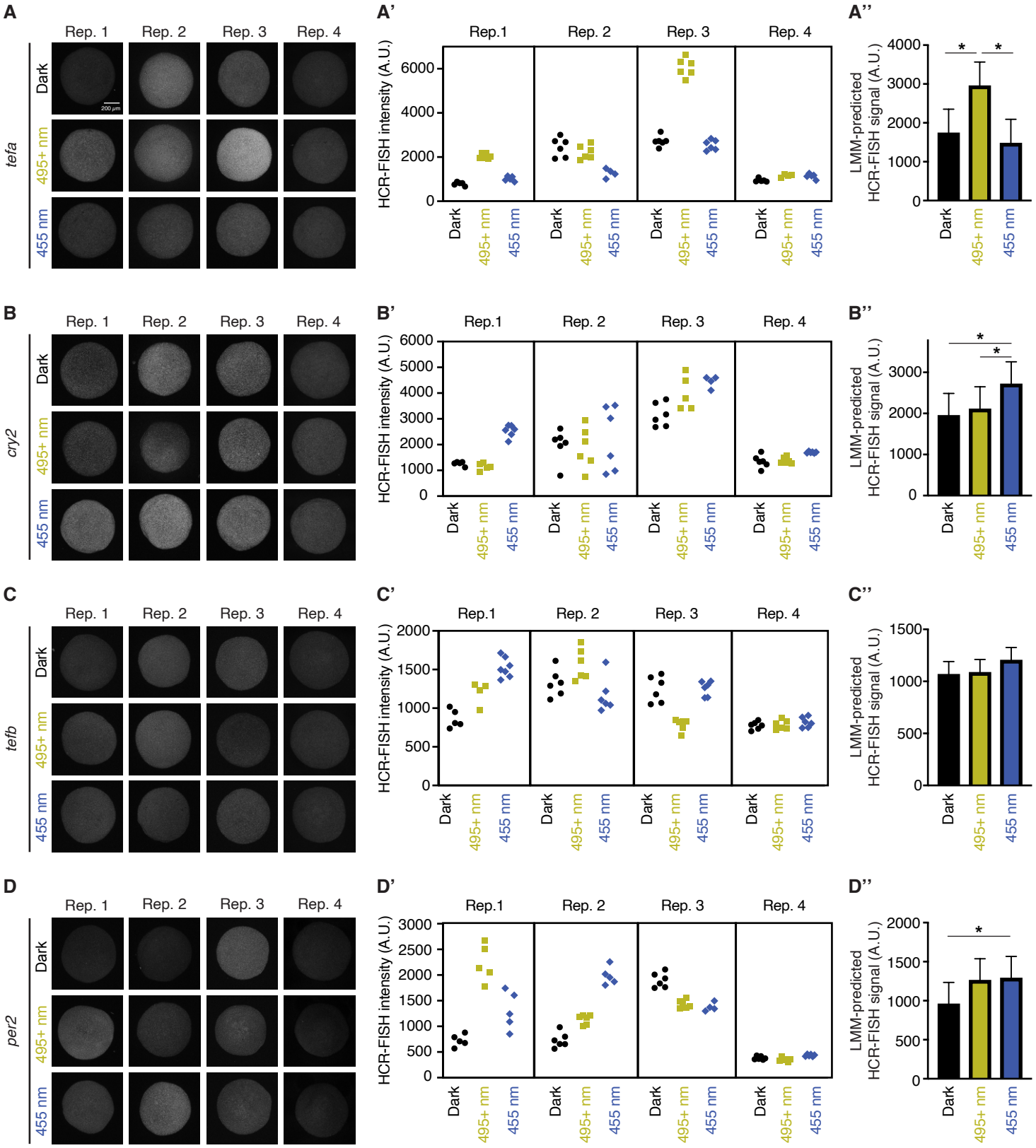


**Supplementary Figure 12: Circadian gene responses to light exposure in gasturation stage embryos. A-D)** Uninjected AB wild type zebrafish embryos were reared in the dark. At early gastrulation (shield stage), a subset of embryos were exposed to 495+ nm light (18.51 W/m$^2$) or 455 nm light (50 W/m$^2$) for 30 min, then dark for 20 min. A third set of embryos were maintained in the dark throughout the experiment. HCR-FISH was performed for the indicated circadian-related genes. Each panel represents four experimental repeats for the indicated gene. (Scale bar is 200 $\mu$m). **A'-D')** Mean HCR-FISH intensities from experiments shown in A-D. Each symbol represents mean intensity from one embryo. **A''-D'')** Quantification of experiments shown in A-D. Linear-mixed model-predicted least squared means of HCR-FISH signal +/- SEM (N = 4; LMM - Fixed Effect: Wavelength, Random Effect: Replicate; post hoc Tukey's HSD where * indicates $p < 0.05$).